Article

Elucidating Drug-Like Compounds and Potential Mechanisms of Corn Silk (*Stigma Maydis*) against Obesity: A Network Pharmacology Study

Ki-Kwang Oh [ID], Md. Adnan [ID] and Dong-Ha Cho *

Department of Bio-Health Convergence, College of Biomedical Science, Kangwon National University, Chuncheon 24341, Korea; nivirna07@kangwon.ac.kr (K.-K.O.); mdadnan1991.pharma@gmail.com (M.A.)
* Correspondence: chodh@kangwon.ac.kr; Tel.: +82-33-250-6475

Abstract: Corn silk (*Stigma Maydis*) has been utilized as an important herb against obesity by Chinese, Korean, and Native Americans, but its phytochemicals and mechanisms(s) against obesity have not been deciphered completely. This study aimed to identify promising bioactive constituents and mechanism of action(s) of corn silk (CS) against obesity via network pharmacology. The compounds from CS were identified using Gas Chromatography Mass Spectrometry (GC-MS) and were confirmed ultimately by Lipinski's rule via SwissADME. The relationships of the compound-targets or obesity-related targets were confirmed by public bioinformatics. The signaling pathways related to obesity, protein-protein interaction (PPI), and signaling pathways-targets-bioactives (STB) were constructed, visualized, and analyzed by RPackage. Lastly, Molecular Docking Test (MDT) was performed to validate affinity between ligand(s) and protein(s) on key signaling pathway(s). We identified a total of 36 compounds from CS via GC-MS, all accepted by Lipinski's rule. The number of 36 compounds linked to 154 targets, 85 among 154 targets related directly to obesity-targets (3028 targets). Of the final 85 targets, we showed that the PPI network (79 edges, 357 edges), 12 signaling pathways on a bubble chart, and STB network (67 edges, 239 edges) are considered as therapeutic components. The MDT confirmed that two key activators (β-Amyrone, β-Stigmasterol) bound most stably to PPARA, PPARD, PPARG, FABP3, FABP4, and NR1H3 on the PPAR signaling pathway, also, three key inhibitors (Neotocopherol, Xanthosine, and β-Amyrone) bound most tightly to AKT1, IL6, FGF2, and PHLPP1 on the PI3K-Akt signaling pathway. Overall, we provided promising key signaling pathways, targets, and bioactives of CS against obesity, suggesting crucial pharmacological evidence for further clinical testing.

Keywords: corn silk (*Stigma Maydis*); obesity; network pharmacology; PPAR signaling pathway; PI3K-Akt signaling pathway

1. Introduction

Obesity is a serious health issue worldwide because it is involved in the main causes of comorbidity and mortality, including diabetes, hypertension, heart failure, atherosclerosis, and some cancers [1,2]. Obesity is characterized by the accumulation of excessive adipose tissues in the body, leading to energy imbalance, alteration of appetite hormones, and insulin resistance [3,4]. Clinically, the criteria of obesity is the that Body Mass Index (BMI) is equal to 30.0 or higher [5]. Obesity can present at all ages, globally, a report announced that the number of overweight and obese individuals will be projected to be 1.35 billion and 573 million by 2030 [6,7].

The most optimal therapeutic strategy against obesity is to inhibit the accumulation of fat in the body as well as to suppress the appetite with special medication [8,9]. At present, a representative drug of anti-obesity is Orlistat (PubChem ID: 3034010), used to decrease the absorption of fatty acid in intestine by inhibiting gastric and pancreatic lipase [10]. In addition, some medications (diethylpropion, fenfluramine, sibutramine,

rimonabant) with appetite suppression efficacy have been prescribed to alleviate obesity in most countries [11]. However, most anti-obesity drugs have serious adverse events such as steatorrhea, flatulence, headache, and hypoglycemia [12]. Natural herbal plants are good resources with less side effects, compared to synthetic drugs [13]. Most recently, osmotin is characterized by a natural plant protein with antifungal efficacy, which is homologous functionally to adiponectin for preventing an excess of fatty acids in the body [14,15]. However, even though these are derived from herbal plants, protein drugs are susceptible to degradation and are not given orally due to poor bioavailability [16]. Some anti-obesity natural organic small compounds (<500 g/mol) have been isolated from marine sponges: Palinurin (from *Ircinia variabilis*) [17], Dysidine (from *Dysidea villosa*) [18], Questinol and citreorosein (from *Stylissa flabelliformis*) [19], and Phorbaketal A (from *Phorbas* sp.) [20]. Other resources are land herbal plants with diverse anti-obesity organic small compounds: Curcumin (from *Curcuma longa* rhizome), Carnosic acid and carnosol (from *Salvia officinalis* leaves), Epigallocatechin 3-O gallate (from *Camellia sinensis*), Ursolic acid (from *Actinidia arguta* root), and Crocetin and crocin (from *Gardenia jasminoides* fruits) [21]. Currently, the majority of drug candidates in herbal plants are dependent on their main parts such as leaves, roots, and fruits. On the other hand, we suggest that medicinal utilization of agricultural substances is a good approach to identify their value. Of these, a report demonstrated that some flavonoids and phenolics from the 50% ethanolic corn silk (CS) extracts have potent anti-obesity efficacy, leading to anti-adipogenesis and lipolysis [22]. However, commonly, bioavailability improvement of phenolic compounds including flavonoids should be applied to accomplish pharmacological functions through leading-edge delivery system [23]. From this point of view, we need to establish a new methodology and concept to analyze anti-obesity on CS. At present, drug-like compound(s), target(s), and signaling pathway(s) of CS against obesity have not been reported. Thus, the studies on drug-like compounds and promising mechanism(s) of CS against obesity should be strengthened to provide pharmacological evidence to support its therapeutic application in alleviating obesity. Network pharmacology is a significant methodology to elucidate multiple components such as signaling pathways, targets, and compounds [24]. Network pharmacology is a key to decipher multiple targets of herbal bioactive compounds [25]. With the rapid progression of network pharmacology, the unveiling of interaction between multi-components and multi-targets gives us a clue to illustrate pathogenesis [26]. Moreover, the network pharmacology analysis in holistic perspectives is an effective approach to develop compounds for the treatment of metabolic disorders such as diabetes mellitus (DM), and obesity [25]. The aim of this study is to investigate the signaling pathways, targets, and compounds of CS against obesity. Firstly, compounds from ethanolic CS extract have been identified by Gas Chromatography-Mass Spectrometry (GC-MS) and screened by Lipinski's rule to identify Drug Like Compounds (DLCs). Then, targets related to DLCs or obesity collected using public bioinformatics, and overlapping targets between DLCs and obesity targets were identified. Secondly, the protein-protein interaction (PPI) based on overlapping targets was constructed by RPackage. Next, a bubble chart used to visualize the Rich factor on overlapping targets was built by RPackage. Thirdly, relationships between signaling pathways, targets, and DLCs were visualized by RPackage. Finally, Molecular Docking Test (MDT) was performed to understand the best affinity between targets and DLCs on key signaling pathways. The concise workflow is exhibited in Figure 1.
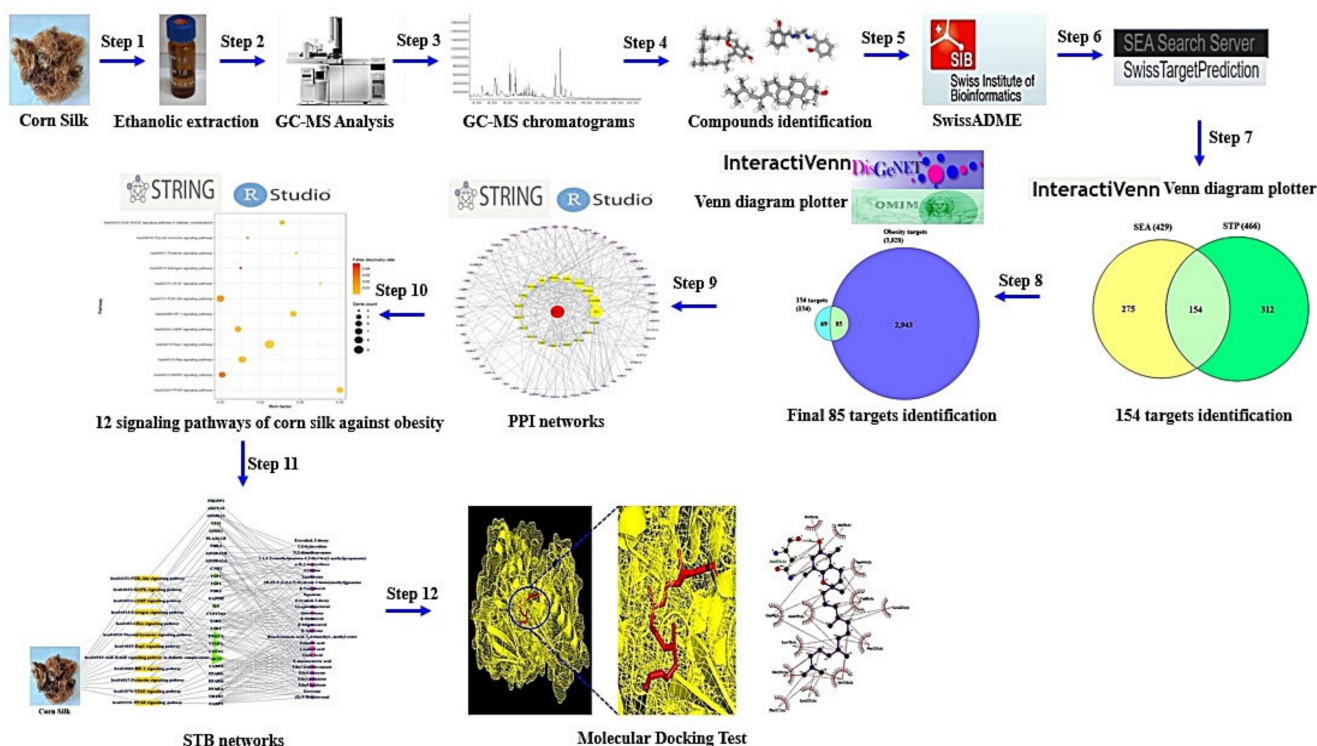
Figure 1. Research process of network pharmacology analysis of CS against obesity.

2. Materials and Methods

2.1. Plant Material and Extracts Preparation

Corn silk (CS) were collected from (latitude: 36.683084, longitude: 128.512617), Gyeongsangbuk-do, Korea, in July 2021. The CS were dried in a shady zone at room temperature (20–22 °C) for 7 days, and dried CS powder was made using an electric blender. Approximately 20 g of CS powder was soaked in 1000 mL of 100% ethyl alcohol (Daejung, Siheung city, Gyeonggi-do, Korea) for 15 days and repeated 3 times to achieve a high yield rate. The solvent extract was collected, filtered with Whatman filter paper No. 1 (Whatman, Model no. WF1-1850, UK Maidstone) and evaporated using a vacuum evaporator (IKA- RV8, Staufen city, Germany) at 40 °C. The yield after evaporating was 1.98 g (Yield rate: 0.99%), which was calculated as follows:

$$\text{Yield (\%)} = (\text{Dried CS weight/Evaporated extraction weight}) \times 100$$

2.2. GC-MS Analysis Condition

Agilent 7890A (Agilent, Santa Clara, CA, USA) was used to perform GC-MS analysis. GC was equipped with a DB-5 (30 m × 0.25 mm × 0.25 µm) capillary column (Agilent, Santa Clara, CA, USA). Initially, the instrument was maintained at a temperature of 100 °C for 2.1 min. The temperature rose to 300 °C at a rate of 25 °C/min and was maintained for 20 min. Injection port temperature and helium flow rate were ensured as 250 °C and 1.5 mL/min, respectively. The ionization voltage was 70 eV. The samples were injected in split mode at 10:1. The MS scan range was set at 35–900 (m/z). The fragmentation patterns of mass spectra were compared with those stored in the W8N05ST Library MS database (analyzed 7 September 2021). The percentage of each compound was calculated from the relative peak area of each compound in the chromatogram [27].

2.3. GC-MS Compounds in CS and Screening of DLCs

The chemical constituents in CS were detected via GC-MS analysis, which were input into PubChem (https://pubchem.ncbi.nlm.nih.gov/, accessed on 9 September 2021) to

identify SMILES (Simplified Molecular Input Line Entry System) format. The screening of DLCs is based on Lipinski's rule via SwissADME (http://www.swissadme.ch/) (accessed on 9 September 2021). Additionally, topological polar surface area (TPSA) to measure cell permeability of compounds was identified by SwissADME (http://www.swissadme.ch/, accessed on 9 September 2021). Commonly, its cut-off value to evaluate cell permeability is typically less than 140 $Å^2$ [28].

2.4. Identification of Target Proteins Associated with Bioactives or Obesity

The bioactives confirmed by Lipinski's rule put the SMILE format into two two public cheminformatics: Similarity Ensemble Approach (SEA) (accessed on 10 September 2021) [29] and SwissTargetPrediction (STP) (accessed on 10 September 2021) [30] with "*Homo Sapiens*" mode. The relationship between target proteins and bioactives were obtained by the two cheminformatics, which demonstrated their use as significant tools to be validated experimentally: A total of 80% out of the novel drug candidates line up with the SEA result, and the promising target proteins of cudraflavone C were identified through STP, thereby, its biological activities were validated by the experiment [31,32]. Altogether, we confirmed that novel potential ligands and target proteins would be identified using the validated data. The target proteins related to obesity were collected by two public bioinformatics DisGeNET (https://www.disgenet.org/search, accessed on 13 September 2021) and OMIM (https://www.ncbi.nlm.nih.gov/omim) (accessed 13 September 2021). The overlapping target proteins between DLCs from CS and obesity-related target proteins were identified and visualized on InteractiVenn [33]. Then, we visualized it on Venn Diagram Plotter.

2.5. PPI Construction of Final Target Proteins and Identification of Rich Factor

The interaction of the final overlapping target proteins was identified by STRING analysis (https://string-db.org/, accessed 14 September 2021) [34]. The number of nodes and edges were identified by PPI construction and thus, signaling pathways involved in overlapping target proteins were explicated by the RPackage bubble chart illustration. On the bubble chart, two key signaling pathways of CS against obesity were finalized.

2.6. The Construction of STB Network

The STB networks were visualized as a size map, based on a degree of value. In the network map, green rectangles (nodes) represented the signaling pathways; yellow triangles (nodes) represented the target proteins; red circles (nodes) represented the bioactives. The size of the yellow triangles stood for the number of relationships with signaling pathways; the size of red circles stood for the number of relationships with target proteins. The assembled network was constructed by utilizing RPackage.

2.7. Bioactives and Target Proteins Preparation for MDT

The bioactives related to the two key signaling pathways were converted. sdf from PubChem into. pdb format utilizing Pymol, and thus they were converted into. pdbqt format via Autodock. The number of the six proteins on the PPAR signaling pathway, i.e., PPARA (PDB ID: 3SP6), PPARD (PDB ID: 5U3Q), PPARG (PDB ID: 3E00), FABP3 (PDB ID: 5HZ9), FABP4 (PDB ID: 3P6D), and NR1H3 (PDB ID: 2ACL), and the number of the seven proteins on PI3K-Akt signaling pathway, i.e., AKT1 (PDB ID: 3O96), IL6 (PDB ID: 4NI9), VEGFA (PDB ID: 3V2A), PRKCA (PDB ID: 3IW4), FGF1 (PDB ID: 3OJ2), FGF2 (PDB ID: 1IIL), and PHLPP1 (not available in the PDB) were identified on STRING via RCSB PDB (https://www.rcsb.org/, accessed 16 September 2021). The proteins were chosen as. PDB format were converted into. pdbqt through Autodock (http://autodock.scripps.edu, accessed on 17 September 2021).

2.8. MDT of Bioactives on Target Proteins Related to Two Key Signaling Pathways

The ligand molecules were docked with target proteins using autodock4 by setting-up 4 energy range and 8 exhaustiveness as default to obtain 10 different poses of ligand molecules [35]. The center of each target protein on PPAR signaling pathway was PPARA (x = 8.006, y = −0.459, z = 23.392)), PPARD (x = 39.265, y = −18.736, z = 119.392), PPARG (x = 2.075, y = 31.910, z = 18.503), FABP3 (x = −1.215, y = 46.730, z = −15.099), FABP4 (x = 7.693, y = 9.921, z = 14.698).

The center of each target protein on PI3K-Akt signaling pathway was Akt1 (x = 6.313, y = −7.926, z = 17.198), IL6 (x = 11.213, y = 33.474, z = 11.162), VEGFA (x = 38.009, y = −10.962, z = 12.171), PRKCA (x = −14.059, y = 38.224, z = 32.319), FGF1 (x = 9.051, y = 22.527, z = −0.061), FGF2 (x = 26.785, y = 14.360, z = −1.182), PHLPP1 (x = −3.881, y = 1.398, z = 2.661). The active site's grid box size was x = 40 Å, y = 40 Å, z = 40 Å. The detailed information of 2D binding was identified by LigPlot+ 2.2 (https://www.ebi.ac.uk/thornton-srv/software/LigPlus/, accessed 18 September 2021) [36]. After MDT, bioactives with the lowest Gibbs free energy were selected to depict the bioactive-protein complex in Pymol.

3. Results

3.1. Physicochemical Properties of Chemical Compounds from Corn Silk (CS)

A total of 36 chemical compounds from CS were detected through GC-MS analysis (Figure 2), and compound name, retention time, peak area, PubChem ID, and taxonomic classification are presented in Table 1. All 36 chemical compounds were accepted by Lipinski's rule (Molecular Weight ≤ 500 g/mol; Moriguchi octanol-water partition coefficient ≤ 4.15; Number of Nitrogen or Oxygen ≤ 10; Number of NH or OH ≤ 5), including TPSA value (< 140 Å^2) (Table 2).
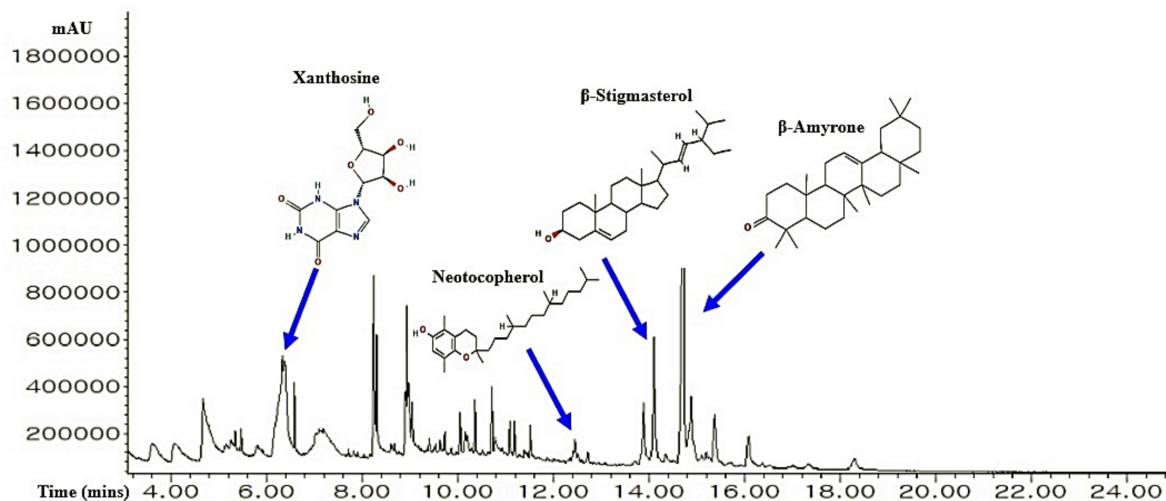
Figure 2. A typical GC-MS peaks of CS ethanolic extract and the number of four key bioactives.

Table 1. A list of the detected 36 bioactives from CS through GC-MS.

No.	Compounds	PubChem ID	RT (mins)	Area (%)	Taxonomic Compound Classification
1	Ethylamine	6341	3.625	2.37	Amines
2	cis-2,3-Epoxybutane	92162	4.097	2.77	Epoxides
3	5-Hydroxymethylfurfural	237332	4.683	8.2	Carbonyl compounds
4	Mannitan	10909888	5.135	0.36	Tetrahydrofurans

Table 1. *Cont.*

No.	Compounds	PubChem ID	RT (mins)	Area (%)	Taxonomic Compound Classification
5	5-Aminovaleric acid	138	5.164	0.67	Amino acids, peptides, and analogues
6	Nitrous acid, 1-methylpropyl ester	13544	5.270	1.18	Organic nitroso compounds
7	Formicin	69365	5.356, 5.481	1.76	Carboxylic acid derivatives
8	Diethyl acetal	7765	5.818	1.39	Ethers
9	Xanthosine	64959	6.337	7.91	Purine nucleosides
10	Cytidine	6175	6.395	6.33	Pyrimidine nucleosides
11	2,4,4-Trimethylpentane-1,3-diyl bis(2-methylpropanoate)	93439	6.606	1.33	Dicarboxylic acids and derivatives
12	α-D-2-deoxyribose	441475	7.116	3.4	Oxanes
13	2R,3S-9-[1,3,4-Trihydroxy-2-butoxymethyl]guanine	135789714	7.193	3.51	Purines and purine derivatives
14	Palmitic acid	985	8.250, 8.616	5.2	Fatty acids and conjugates
15	Ethyl palmitate	12366	8.318	3.35	Fatty acid esters
16	Linoleic acid	5280450	8.914	1.85	Lineolic acids and derivatives
17	Ethyl linoleate	5282184	8.952	4.24	Lineolic acids and derivatives
18	Ethyl stearate	8122	9.058	1.41	Fatty acid esters
19	Estradiol, 3-deoxy	537293	9.414	0.74	Estrane steroids
20	Oleic Acid	445639	9.645	0.59	Fatty acids and conjugates
21	Ethyl isovalerate	7945	9.731	0.76	Fatty acid esters
22	Eicosane	8222	10.058, 10.721, 11.529	2.71	Alkanes
23	(Z)-9-Hexadecenal	5364643	10.164	1.61	Fatty aldehydes
24	Heneicosanoic acid, 2,4-dimethyl-, methyl ester	560463	10.366	1.29	Fatty acid esters
25	7-Pentadecyne	549063	10.789	1.32	Acetylenes
26	Ethyl heptadecanoate	26397	11.096	0.9	Fatty acid esters
27	Squalene	638072	11.193	0.76	Triterpenoids
28	1,3-Dioxolane, 4-ethyl-5-octyl-2,2-bis(trifluoromethyl)-, trans-	91694992	12.423	0.24	Ethers
29	Neotocopherol	86052	12.462	0.74	1-hydroxy-4-unsubstituted benzenoids
30	N,2-diaminopropane	7210	12.731, 14.356	1.02	1-hydroxy-4-unsubstituted benzenoids
31	24-epicampesterol	5283637	13.895	2.85	Ergostane steroids
32	β-Stigmasterol	6432745	14.116	5.32	Stigmastanes and derivatives
33	β-Sitosterol	222284	14.721	12.41	Triterpenoids
34	β-Amyrone	612782	14.895, 15.385	6.95	Triterpenoids
35	Sitostenone	5484202	16.087	1.64	Stigmastanes and derivatives
36	2-Ethylacridine	610161	18.308	0.91	Benzoquinolines

Table 2. Physicochemical properties of 36 bioactives for Lipinski's rule, bioavailability, and cell membrane permeability.

No.	Compounds	Lipinski Rules				Lipinski's Violations	Bioavailability Score	TPSA(Å²)
		MW	HBA	HBD	MLog P			
		<500	<10	≤5	≤4.15	≤1	>0.1	<140
1	Ethylamine	45.08	1	1	−0.23	0	0.55	26.02
2	cis-2,3-Epoxybutane	72.11	1	0	0.35	0	0.55	12.53
3	5-Hydroxymethylfurfural	126.11	3	1	−1.06	0	0.55	50.44
4	Mannitan	164.16	5	4	−2.35	0	0.55	90.15
5	5-Aminovaleric acid	117.15	3	2	0.01	0	0.55	63.32

Table 2. *Cont.*

No.	Compounds	Lipinski Rules				Lipinski's Violations	Bioavailability Score	TPSA(Å²)
		MW	HBA	HBD	MLog P			
		<500	<10	≤5	≤4.15	≤1	>0.1	<140
6	Nitrous acid, 1-methylpropyl ester	103.12	3	0	0.42	0	0.55	38.66
7	Formicin	89.09	2	2	−0.85	0	0.55	49.33
8	Diethyl acetal	118.17	2	0	1.01	0	0.55	18.46
9	Xanthosine	284.23	7	5	−2.30	0	0.55	153.46
10	Cytidine	243.22	6	4	−2.29	0	0.55	130.83
11	2,4,4-Trimethylpentane-1,3-diyl bis(2-methylpropanoate)	286.41	4	0	3.17	0	0.55	52.60
12	α-D-2-deoxyribose	134.13	4	3	−1.49	0	0.55	69.92
13	2R,3S-9-[1,3,4-Trihydroxy-2-butoxymethyl] guanine	285.26	7	5	−2.76	0	0.55	159.51
14	Palmitic acid	256.42	2	1	4.19	1	0.85	37.30
15	Ethyl palmitate	284.48	2	0	4.67	1	0.55	26.30
16	Linoleic acid	280.45	2	1	4.47	1	0.85	37.30
17	Ethyl linoleate	308.50	2	0	4.93	1	0.55	26.30
18	Ethyl stearate	312.53	2	0	5.13	1	0.55	26.30
19	Estradiol, 3-deoxy	256.38	1	1	4.19	1	0.55	20.23
20	Oleic Acid	282.46	2	1	4.57	1	0.85	37.30
21	Ethyl isovalerate	130.18	2	0	1.63	0	0.55	26.30
22	Eicosane	282.55	0	0	7.38	1	0.55	0.00
23	(Z)-9-Hexadecenal	238.41	1	0	4.20	1	0.55	17.07
24	Heneicosanoic acid, 2,4-dimethyl-, methyl ester	368.64	2	0	6.00	1	0.55	26.30
25	7-Pentadecyne	208.38	0	0	6.04	1	0.55	0.00
26	Ethyl heptadecanoate	298.50	2	0	4.91	1	0.55	26.30
27	Squalene	410.72	0	0	7.93	1	0.55	0.00
28	1,3-Dioxolane, 4-ethyl-5-octyl-2,2-bis(trifluoromethyl)-, trans-	350.34	8	0	4.02	0	0.55	18.46
29	Neotocopherol	416.68	2	1	5.94	1	0.55	29.46
30	N,2-diaminopropane	282.34	5	4	1.81	0	0.55	65.18
31	24-epicampesterol	400.68	1	1	6.54	1	0.55	20.23
32	β-Stigmasterol	412.69	1	1	6.62	1	0.55	20.23
33	β-Sitosterol	414.71	1	1	6.73	1	0.55	20.23
34	β-Amyrone	424.70	1	0	6.82	1	0.55	17.07
35	Sitostenone	412.69	1	0	6.62	1	0.55	17.07
36	2-Ethylacridine	207.27	1	0	3.58	0	0.55	12.89

3.2. Identification of Overlapping Target Proteins between SEA and STP Linked to 36 Compounds

A total of 429 target proteins from SEA and 466 target proteins from STP linked to the abovementioned 36 compounds were identified through SMILES format (Supplementary Table S1). The results of the Venn diagram exhibited that 154 overlapping target proteins were overlapped between SEA and STP public databases (Supplementary Table S1) (Figure 3A).
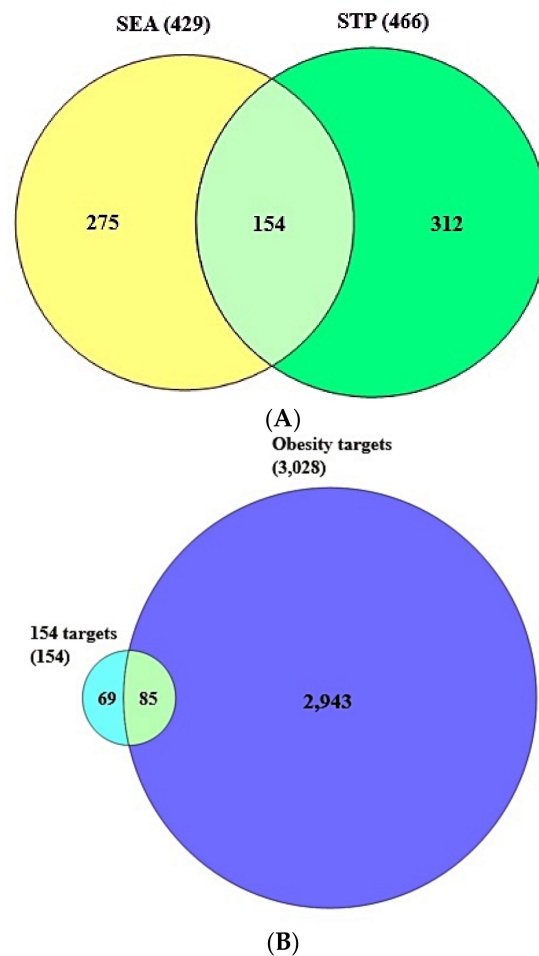
Figure 3. (**A**) A total of 154 overlapping targets between SEA (429 targets) and STP (466 targets). (**B**) A total of 85 final targets between the 154 overlapping targets and obesity-related targets (3028 targets).

3.3. The Final Overlapping Target Proteins between Obesity-Related Target Proteins and the 154 Overlapping Target Proteins

As shown in Supplementary Table S2, a total of 3028 target proteins associated with obesity were retrieved by DisGeNet and OMIM databases. The Venn diagram displayed that a total of 85 target proteins overlapped between obesity related to 3028 target proteins and 154 overlapping target proteins (Supplementary Table S2) (Figure 3B).

3.4. Protein-Protein Interaction (PPI) from Final 85 Target Proteins

Using STRING analysis, 79 out of 85 target proteins were correlated closely with each other with 79 nodes and 357 edges (Figure 4). The eliminated 6 target proteins (RNASE2, SLC22A6, GSTK1, PAM, OXER1, and THRA) did not interact with the 85 target proteins. In the PPI network, the AKT1 target protein had the greatest degree of centrality (43) and was considered as the hub target protein (Table 3).
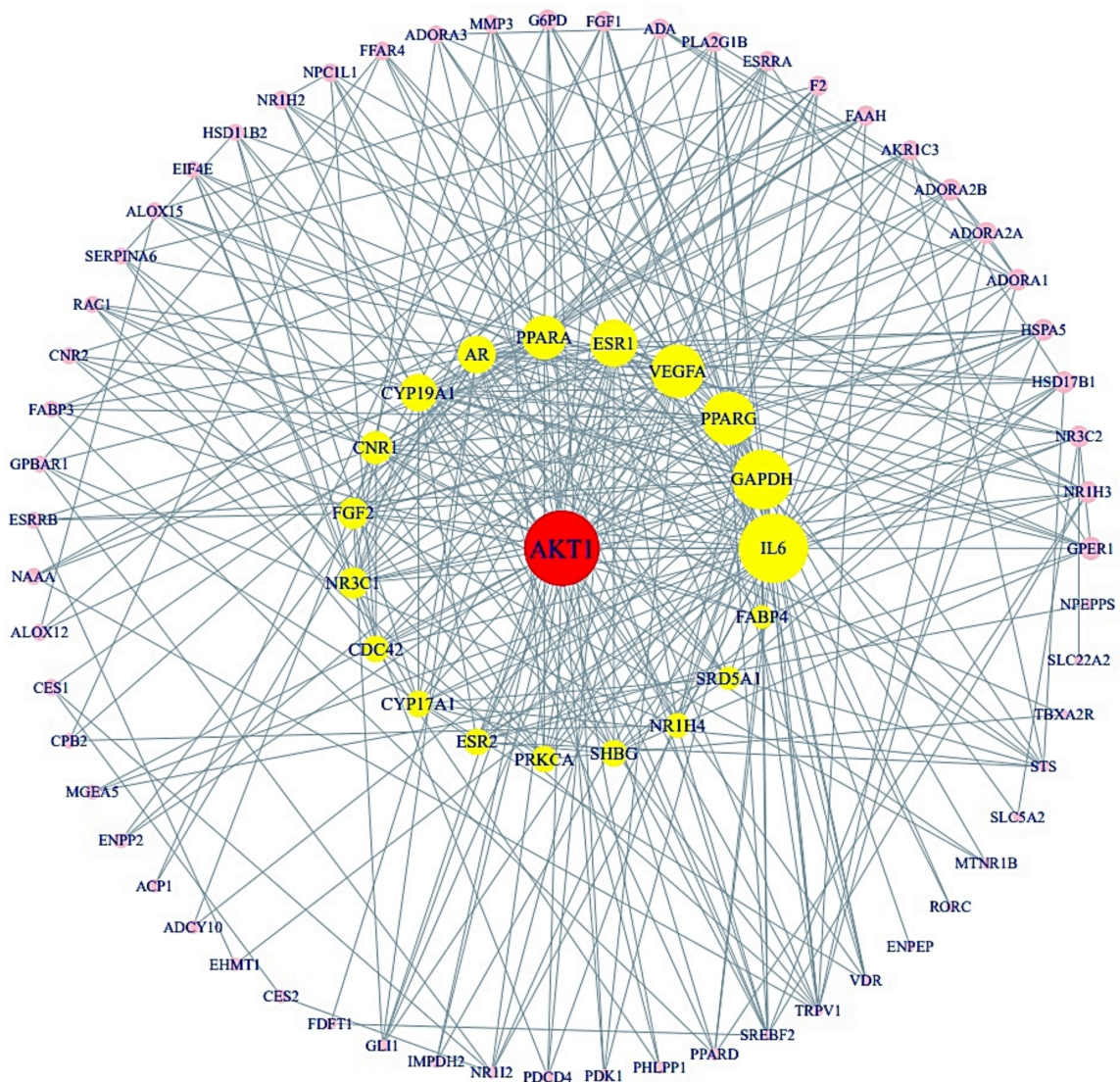
Figure 4. PPI networks (79 nodes, 357 edges). The size of the circle represents degree of values.

Table 3. The degree value of 79 targets in PPI.

No.	Target	Degree of Value	No.	Target	Degree of Value
1	AKT1	43	41	NR1I2	7
2	IL6	39	42	ADORA3	6
3	GAPDH	33	43	ALOX15	6
4	PPARG	29	44	EIF4E	6
5	VEGFA	29	45	FFAR4	6
6	ESR1	25	46	GLI1	6
7	PPARA	23	47	HSD11B2	6
8	AR	19	48	NPC1L1	6
9	CYP19A1	19	49	NR1H2	6
10	CNR1	16	50	RAC1	6
11	FGF2	15	51	SERPINA6	6
12	NR3C1	15	52	VDR	6
13	CDC42	12	53	PPARD	6
14	CYP17A1	12	54	CNR2	5
15	ESR2	12	55	FABP3	5
16	PRKCA	12	56	GPBAR1	5

Table 3. *Cont.*

No.	Target	Degree of Value	No.	Target	Degree of Value
17	TRPV1	12	57	ESRRB	4
18	SREBF2	11	58	NAAA	4
19	NR1H4	10	59	PDK1	4
20	SHBG	10	60	PDCD4	4
21	SRD5A1	10	61	ALOX12	3
22	FABP4	9	62	CES1	3
23	GPER1	9	63	CPB2	3
24	HSD17B1	9	64	ENPP2	3
25	HSPA5	9	65	MGEA5	3
26	NR1H3	9	66	MTNR1B	3
27	NR3C2	9	67	IMPDH2	3
28	STS	9	68	PHLPP1	3
29	ADORA1	8	69	ACP1	2
30	ADORA2A	8	70	CES2	2
31	ADORA2B	8	71	EHMT1	2
32	AKR1C3	8	72	FDFT1	2
33	ESRRA	8	73	RORC	2
34	F2	8	74	SLC5A2	2
35	FAAH	8	75	TBXA2R	2
36	PLA2G1B	8	76	ADCY10	1
37	ADA	7	77	ENPEP	1
38	FGF1	7	78	NPEPPS	1
39	G6PD	7	79	SLC22A2	1
40	MMP3	7			

3.5. The 12 Signaling Pathways and Identification of Two Key Pathways of CS against Obesity

The results of Kyoto Encyclopedia of Genes and Genomes (KEGG) pathway enrichment analysis showed that 85 target proteins were related directly to 12 signaling pathways (False Discovery Rate < 0.05). The 12 signaling pathways were implicated with occurrence and development of obesity, suggesting that these pathways might be important signaling pathways of CS against obesity. The description of the 12 signaling pathways was represented in Table 4. In addition, a bubble chat suggested that both the PPAR signaling pathway with the highest rich factor and PI3K-Akt signaling pathway with the lowest rich factor might be key signaling pathways of CS against obesity (Figure 5).

Table 4. Targets in 12 signaling pathways enrichment associated with obesity.

KEGG ID	Targets	False Discovery Rate
hsa03320:PPAR signaling pathway	PPARA, PPARD, PPARG, FABP3, FABP4, NR1H3	0.0001200
hsa04370:VEGF signaling pathway	AKT1, VEGFA, PRKCA, CDC42	0.0049000
hsa04917:Prolactin signaling pathway	AKT1, ESR1, ESR2, CYP17A1	0.0080000
hsa04066:HIF-1 signaling pathway	AKT1, IL6, GAPDH, VEGFA, PRKCA, PDK1	0.0006900
hsa04933:AGE-RAGE signaling pathway in diabetic complications	AKT1, IL6, VEGFA, PRKCA, CDC42	0.0035000
hsa04015:Rap1 signaling pathway	AKT1, VEGFA, CDC42, PRKCA, FGF1, FGF2, CNR1, ADRA2A, ADORA2B	0.0000376
hsa04919:Thyroid hormone signaling pathway	AKT1, PRKCA, ESR1, THRA	0.0337000
hsa04014:Ras signaling pathway	AKT1, VEGFA, CDC42, PRKCA, FGF1, FGF2	0.0031000
hsa04915:Estrogen signaling pathway	AKT1, ESR1, ESR2, GPER1	0.0480000
hsa04024:cAMP signaling pathway	AKT1, PPARA, ADORA2A, GLI1, ADORA1, ADCY10	0.0089000
hsa04010:MAPK signaling pathway	AKT1, VEGFA, CDC42, PRKCA, FGF1, FGF2	0.0328000
hsa04151:PI3K-Akt signaling pathway	AKT1, IL6, VEGFA, PRKCA, FGF1, FGF2, PHLPP1	0.0194000
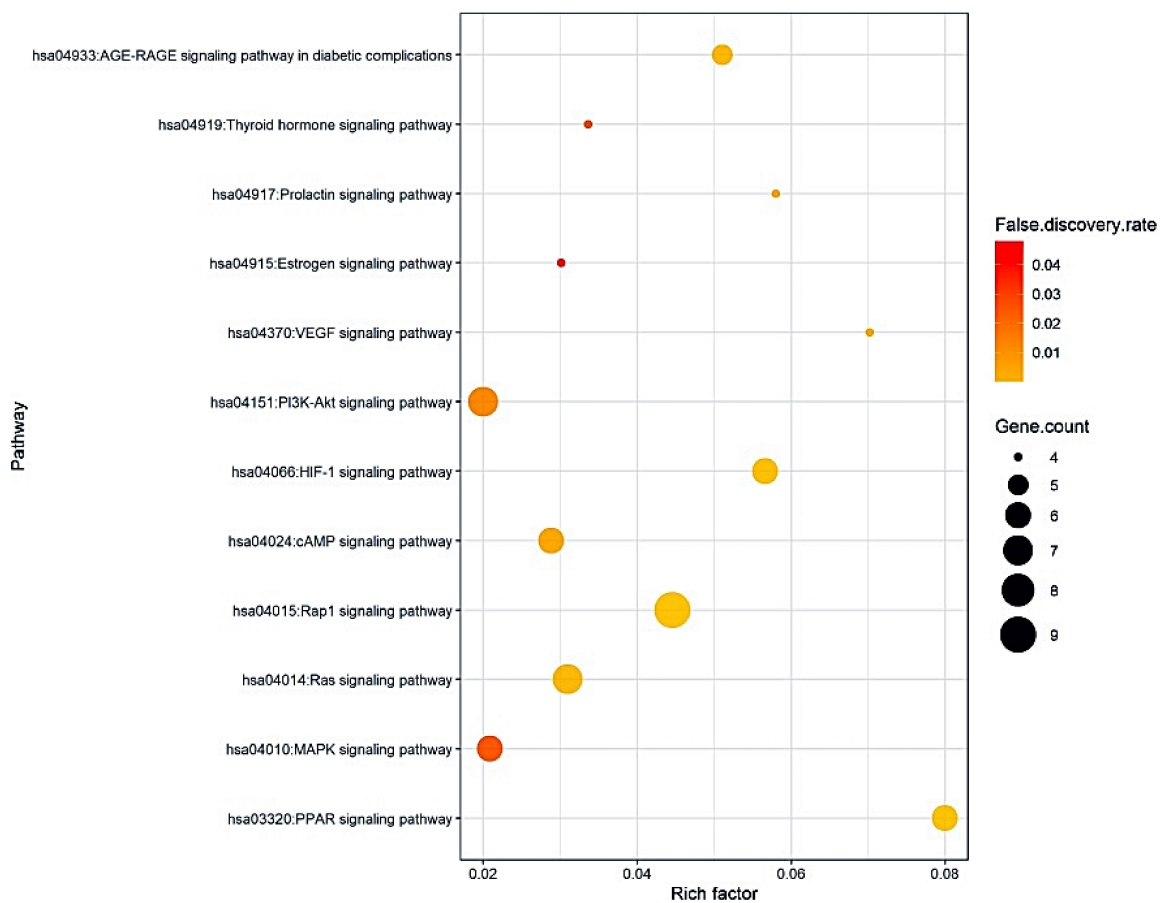
Figure 5. A bubble chart of 12 signaling pathways associated with progression and development of obesity.

3.6. The Construction of a Signaling Pathway-Target Protein-Bioactive (STB) Networks

A signaling pathway-target protein- bioactive (STB) network of CS was exhibited in Figure 6. There were 12 signaling pathways, 28 targets, and 27 bioactives (67 nodes, 239 edges). The nodes stood for a total number of each component: signaling pathways, target proteins, and bioactives. The edges represent relationships of the three components. The STB network indicated that each component of the network is a significant element with therapeutic efficacy against obesity. The AKT1 is the uppermost target with the greatest degree value (11) among 12 signaling pathways (Table 5). Noticeably, a sole signaling pathway not to be connected to AKT1 was the PPAR signaling pathway with the highest rich factor.

Table 5. The degree value of 28 targets in STB.

No.	Target	Degree of Value	No.	Target	Degree of Value
1	AKT1	11	15	PPARG	1
2	PRKCA	8	16	FABP4	1
3	VEGFA	7	17	CYP17A1	1
4	CDC42	5	18	GAPDH	1
5	FGF1	4	19	PDK1	1
6	FGF2	4	20	CNR1	1
7	ESR1	3	21	ADORA2B	1
8	IL6	3	22	THRA	1
9	PPARA	2	23	PLA2G1B	1
10	ESR2	2	24	GPER1	1
11	ADORA2A	2	25	GLI1	1
12	FABP3	1	26	ADORA1	1
13	NR1H3	1	27	ADCY10	1
14	PPARD	1	28	PHLPP1	1
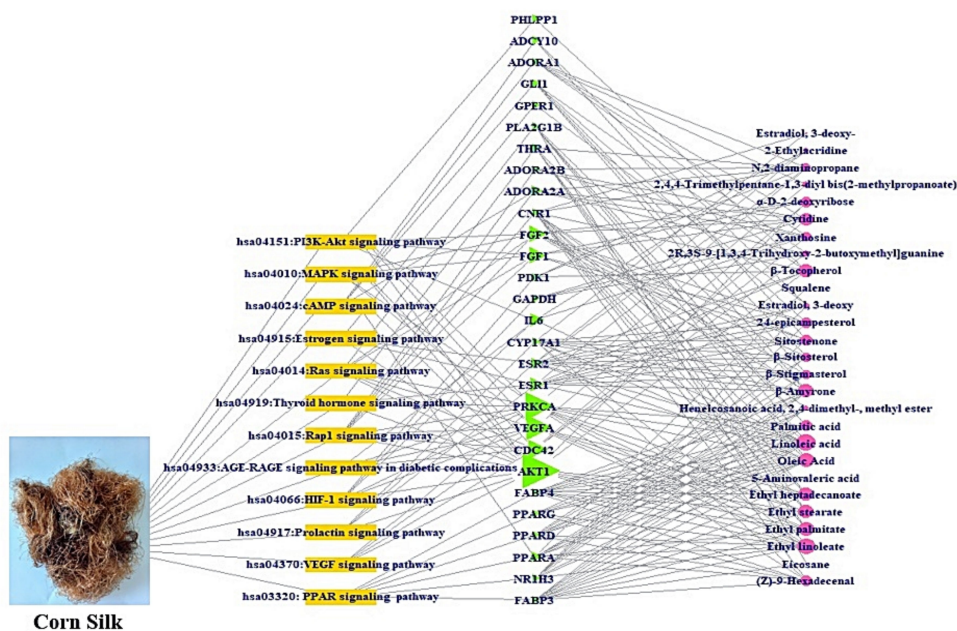
Figure 6. STB networks (67 nodes, 239 edges). Yellow rectangle: signaling pathway; green triangle: target; pink circle: bioactive.

3.7. MDT of 6 Target Proteins, 2 Key Bioactives, and 9 Positive Controls on PPAR Signaling Pathway

Through MDT analysis, it was unveiled that PPARA(PDB ID: 3SP6) was associated with 9 bioactives: (1)β-Amyrone, (2) Squalene, (3) Ethyl palmitate, (4) Heneicosanoic, 2,4-dimethyl-,methyl ester, (5) Oleic acid, (6) Ethyl linoleate, (7) Palmitic acid, (8) Linoleic acid, and (9) (Z)-9-Hexadecenal, PPARD (PDB ID: 5U3Q) was related to 8 bioactives: (1) β-Stigmasterol, (2) β-Sitosterol, (3) Heneicosanoic, 2,4-dimethyl-,methyl ester, (4) Ethyl linoleate, (5) Linoleic acid, (6) Oleic acid, (7) Palmitic acid, and (8) (Z)-9-Hexadecenal, PPARG (PDB ID: 3E00) was connected to 6 bioactives: (1) β-Amyrone, (2) Ethyl linoleate, (3) Linoleic acid, (4) Oleic acid, (5) Palmitic acid, and (6) (Z)-9-Hexadecenal, FABP3 (PDB ID: 5HZ9) was associated with 12 bioactives: (1) β-Amyrone, (2) Heneicosanoic, 2,4-dimethyl-,methyl ester, (3) Eicosane, (4) Ethyl stearate, (5) Ethyl heptacecanoate, (6) Ethyl linoleate, (7) Ethyl palmitate, (8) Linoleic acid, (9) (Z)-9-Hexadecenal, (10) Oleic acid, (11) Palmitic acid, and (12) 5-Aminovaleric acid, FABP4 (PDB ID: 3P6D) was related to 11 bioactives: (1) β-Amyrone, (2) Heneicosanoic, 2,4-dimethyl-,methyl ester, (3) Ethyl stearate, (4) Ethyl palmitate, (5) Ethyl heptacecanoate, (6) Ethyl linoleate, (7) 5-Aminovaleric acid, (8) Oleic acid, (9) Linoleic acid, (10) Palmitic acid, and (11) (Z)-9-Hexadecenal, and NR1H3 (PDB ID: 2ACL) was connected to 9 bioactives: (1) β-Amyrone, (2) β-Stigmasterol, (3) β-Sitosterol, (4) Estradiol, 3-deoxy, (5) Sitostenone, (6) 24-epicampesterol, (7) Ethyl linoleate, (8) Linoleic acid, and (9) Oleic acid.

It was observed that β-Amyrone had the highest affinity on five out of six target proteins: −16.1 kcal/mol on PPARA (PDB ID: 3SP6), −14.0 kcal/mol on PPARG (PDB ID: 3E00), −21.5 kcal/mol on FABP3 (PDB ID: 5HZ9), −13.2 kcal/mol on FABP4 (PDB ID: 3P6D), and −15.4 kcal/mol on NR1H3 (PDB ID: 2ACL). Interestingly, the highest affinity on PPARD (PDB ID: 5U3Q) was β-Stigmasterol with −10.8 kcal/mol. The docking detail information is enlisted in Table 6. Additionally, MDT was performed to compare bioactives with positive controls (Table 7). The results of MDT suggested that β-Amyrone on PPARA (PDB ID: 3SP6), PPARG (PDB ID: 3E00), and NR1H3 (PDB ID: 2ACL) had better affinity than the current positive controls. Moreover, it has been shown that β-Stigmasterol on PPARD (PDB ID: 5U3Q) had greater affinity than Cardarine used as an anti-obesity drug. The other two target proteins were not positive controls compared with β-Amyrone. Collectively, both β-Amyrone and β-Stigmasterol of CS on obesity were potential ligands to activate the PPAR signaling pathway. Its complex figures are depicted in Figure 7.

Table 6. Binding energy and interactions of potential bioactives on the PPAR signaling pathway.

Protein	Ligand	PubChem ID	Binding Energy (kcal/mol)	Grid Box Center	Grid Box Dimension	Hydrogen Bond Interactions Amino Acid Residue	Hydrophobic Interactions Amino Acid Residue
PPARA (PDB ID: 3SP6)	(*) β-Amyrone	612782	−16.1	x = 8.006 y = −0.459 z = 23.392	size_x = 40 size_y = 40 size_z = 40	N/A	Tyr334, Ala333, Val324 Met320, Phe218, Met220 Glu286, Val332, Asn219 Thr279
	Squalene	638072	−6.0	x = 8.006 y = −0.459 z = 23.392	size_x = 40 size_y = 40 size_z = 40	N/A	Tyr334, Asn336, Ala333 Thr279, Leu254, Val332 Ile241, Glu251, Ala250 Cys275, Cys278, Val255
	Ethyl palmitate	12366	−6.0	x = 8.006 y = −0.459 z = 23.392	size_x = 40 size_y = 40 size_z = 40	N/A	Met320, Leu321, Val324 Leu331, Val332, Ala333 Thr279, Tyr334, Asn219 Thr283, Ile317
	Heneicosanoic acid, 2,4-dimethyl-, methyl ester	560463	−5.8	x = 8.006 y = −0.459 z = 23.392	size_x = 40 size_y = 40 size_z = 40	N/A	Lys257, Val255, His274 Leu254, Ala250, Glu251 Ala333, Cys275, Cys278 Leu258
	Oleic Acid	445639	−5.3	x = 8.006 y = −0.459 z = 23.392	size_x = 40 size_y = 40 size_z = 40	N/A	Leu254, Val255, Ala250 Ala333, Asn219, Thr283 Met320, Leu321, Val324 Ile317, Thr279, Tyr334 Cys275, Glu251
	Ethyl linoleate	5282184	−5.0	x = 8.006 y = −0.459 z = 23.392	size_x = 40 size_y = 40 size_z = 40	N/A	Glu282, Tyr334, Thr279 Ala333, Glu251, Leu254 Cys275, Ala250, Val255 Cys278, Val281
	Palmitic acid	985	−4.9	x = 8.006 y = −0.459 z = 23.392	size_x = 40 size_y = 40 size_z = 40	N/A	Val332, Ile241, Ala333 Thr279, Val255, Tyr334 Leu258, Cys275, Ala250 Leu254, Glu251
	Linoleic acid	5280450	−4.9	x = 8.006 y = −0.459 z = 23.392	size_x = 40 size_y = 40 size_z = 40	Ser323, Tyr214	Asn221, Met320, Val324 Met320, Asn219, Tyr334 Thr279, Leu331, Leu321 Thr283, Ile317
	(Z)-9-Hexadecenal	5364643	−3.8	x = 8.006 y = −0.459 z = 23.392	size_x = 40 size_y = 40 size_z = 40	Thr307	Asn303, Lys310, Tyr311 Pro389, Asp466, Ser688 Val306
PPARD (PDB ID: 5U3Q)	(*) β-Stigmasterol	6432745	−10.8	x = 39.265 y = −18.736 z = 119.392	size_x = 40 size_y = 40 size_z = 40	N/A	Ser271, Glu262, Ser271 Pro268, Ser266, Lys265

Table 6. *Cont.*

Protein	Ligand	PubChem ID	Binding Energy (kcal/mol)	Grid Box Center	Grid Box Dimension	Hydrogen Bond Interactions Amino Acid Residue	Hydrophobic Interactions Amino Acid Residue
	β-Sitosterol	222284	−7.1	x = 39.265 y = −18.736 z = 119.392	size_x = 40 size_y = 40 size_z = 40	Arg407, Glu288	Asp439, Tyr284, Pro362 Met440, Val410, Thr411
	Heneicosanoic acid, 2,4-dimethyl-, methyl ester	560463	−5.9	x = 39.265 y = −18.736 z = 119.392	size_x = 40 size_y = 40 size_z = 40	N/A	Met440, Thr411, Val410 Tyr441, Pro362, Asp360 Arg361, Arg407, Tyr284
	Ethyl linoleate	5282184	−5.6	x = 39.265 y = −18.736 z = 119.392	size_x = 40 size_y = 40 size_z = 40	N/A	Met440, Tyr441, Asp439 Pro362, Tyr284, Arg361 Val410, Thr411
	Linoleic acid	5280450	−5.2	x = 39.265 y = −18.736 z = 119.392	size_x = 40 size_y = 40 size_z = 40	N/A	Val410, Arg407, Met440 Asp439, Thr411, Tyr411 Tyr284, Asp360, Pro362 Arg361, Glu288
	Oleic Acid	445639	−4.9	x = 39.265 y = −18.736 z = 119.392	size_x = 40 size_y = 40 size_z = 40	N/A	Asp360, Pro362, Tyr284 Val410, Met440, Tyr441 Thr411
	Palmitic acid	985	−4.6	x = 39.265 y = −18.736 z = 119.392	size_x = 40 size_y = 40 size_z = 40	N/A	Tyr441, Pro362, Arg361 Val410, Tyr284, Glu288 Met440, Thr411, Ala414 Arg407
	(Z)-9-Hexadecenal	5364643	−3.7	x = 39.265 y = −18.736 z = 119.392	size_x = 40 size_y = 40 size_z = 40	Arg361	Thr411, Arg407, Pro362 Asp439, Met440
PPARG (PDB ID: 3E00)	(*) β-Amyrone	612782	−14.0	x = 2.075 y = 31.910 z = 18.503	size_x = 40 size_y = 40 size_z = 40	N/A	Glu343, Glu295, Ile326 Ile296, Ala292, Phe226 Met329, Leu333, Pro227 Leu228
	Ethyl linoleate	5282184	−5.9	x = 2.075 y = 31.910 z = 18.503	size_x = 40 size_y = 40 size_z = 40	N/A	Ile296, Met329, Ile326 Leu228, Leu333, Ala292 Arg288, Phe226, Glu295
	Linoleic acid	5280450	−5.3	x = 2.075 y = 31.910 z = 18.503	size_x = 40 size_y = 40 size_z = 40	Thr162, Leu167	Arg202, Tyr192, Asp166 Lys336, Glu369, Val372 Arg350, Glu351, Gln193 Lys354
	Oleic Acid	445639	−5.1	x = 2.075 y = 31.910 z = 18.503	size_x = 40 size_y = 40 size_z = 40	Asp441, Asn377	Arg426, Lys381, Asp379 Phe370, Lys373, Glu448 Ile445, Pro366, Glu369 Gln444

Table 6. *Cont.*

Protein	Ligand	PubChem ID	Binding Energy (kcal/mol)	Grid Box Center	Grid Box Dimension	Hydrogen Bond Interactions Amino Acid Residue	Hydrophobic Interactions Amino Acid Residue
	Palmitic acid	985	−5.1	x = 2.075 y = 31.910 z = 18.503	size_x = 40 size_y = 40 size_z = 40	Glu291, Arg288	Glu343, Leu333, Leu330 Leu228, Met329, Ala292 Ile326, Glu295
	(Z)-9-Hexadecenal	5364643	−5.0	x = 2.075 y = 31.910 z = 18.503	size_x = 40 size_y = 40 size_z = 40	N/A	Met329, Leu333, Ser332 Leu228, Arg288, Glu295 Glu343, Ala292
FABP3 (PDB ID: 5HZ9)	(*) β-Amyrone	612782	−21.5	x = −1.215 y = 46.730 z = −15.099	size_x = 40 size_y = 40 size_z = 40	N/A	Phe28, Gln32, Lys32 Thr57, Ala29
	Heneicosanoic acid, 2,4-dimethyl-, methyl ester	560463	−8.8	x = −1.215 y = 46.730 z = −15.099	size_x = 40 size_y = 40 size_z = 40	N/A	Glu27, Phe28, Gly25 Ala29, Lys22, Gln32
	Eicosane	8222	−8.6	x = −1.215 y = 46.730 z = −15.099	size_x = 40 size_y = 40 size_z = 40	N/A	Lys22, Thr57, Gln32 Gly25, Phe28, Ala29
	Ethyl stearate	8122	−8.3	x = −1.215 y = 46.730 z = −15.099	size_x = 40 size_y = 40 size_z = 40	N/A	Phe58, Gln32, Gly25 Phe28
	Ethyl heptadecanoate	26397	−8.3	x = −1.215 y = 46.730 z = −15.099	size_x = 40 size_y = 40 size_z = 40	N/A	Gly27, Gln32, Ala29 Phe28
	Ethyl linoleate	5282184	−8.2	x = −1.215 y = 46.730 z = −15.099	size_x = 40 size_y = 40 size_z = 40	N/A	Lys22, Ala29, Phe28 Gly25, Gln32
	Ethyl palmitate	12366	−8.2	x = −1.215 y = 46.730 z = −15.099	size_x = 40 size_y = 40 size_z = 40	N/A	Ala29, Gln32, Phe28 Gly25, Gly27, Lys22
	Linoleic acid	5280450	−7.4	x = −1.215 y = 46.730 z = −15.099	size_x = 40 size_y = 40 size_z = 40	Lys22	Ala29, Gln32, Phe28 Gly25, Gly27
	(Z)-9-Hexadecenal	5364643	−6.9	x = −1.215 y = 46.730 z = −15.099	size_x = 40 size_y = 40 size_z = 40	N/A	Gly27, Gly25, Gln32 Ala29, Phe28, Ala29
	Oleic Acid	445639	−6.9	x = −1.215 y = 46.730 z = −15.099	size_x = 40 size_y = 40 size_z = 40	N/A	Phe28, Gly27, Ala29 Gln32

Table 6. *Cont.*

Protein	Ligand	PubChem ID	Binding Energy (kcal/mol)	Grid Box		Hydrogen Bond Interactions	Hydrophobic Interactions
				Center	Dimension	Amino Acid Residue	Amino Acid Residue
	Palmitic acid	985	−6.5	x = −1.215 y = 46.730 z = −15.099	size_x = 40 size_y = 40 size_z = 40	N/A	Val33, Gln32, Ala29 Phe58, Lys22, Thr57
	5-Aminovaleric acid	138	−5.1	x = −1.215 y = 46.730 z = −15.099	size_x = 40 size_y = 40 size_z = 40	Ala29, Phe28, Val26	Gly25, Gly27, Lys22 Phe28
FABP4 (PDB ID: 3P6D)	(*) β-Amyrone	612782	−13.2	x = 7.693 y = 9.921 z = 14.698	size_x = 40 size_y = 40 size_z = 40	N/A	Val90, Lys107, Glu109 Glu116, Val114, Lys105
	Heneicosanoic acid, 2,4-dimethyl-, methyl ester	560463	−5.6	x = 7.693 y = 9.921 z = 14.698	size_x = 40 size_y = 40 size_z = 40	Leu86	Leu66, Ile49, Asp47 Cys1, Ser1, Met0
	Ethyl stearate	8122	−5.5	x = 7.693 y = 9.921 z = 14.698	size_x = 40 size_y = 40 size_z = 40	Gly88	Asp87, Leu86, Asp47 Leu66, Gly46, Ile49 Val44, Ser1, Cys1 Met0
	Ethyl palmitate	12366	−5.4	x = 7.693 y = 9.921 z = 14.698	size_x = 40 size_y = 40 size_z = 40	N/A	Ala29, Gln32, Phe28 Gly25, Gly27, Lys22
	Ethyl heptadecanoate	26397	−5.3	x = 7.693 y = 9.921 z = 14.698	size_x = 40 size_y = 40 size_z = 40	Gly88	Asp87, Leu86, Asp47 Ile49, Ser1, Leu66 Cys1, Met0
	Ethyl linoleate	5282184	−5.2	x = 7.693 y = 9.921 z = 14.698	size_x = 40 size_y = 40 size_z = 40	Gly88	Asp87, Met0, Ile49 Cys1, Gly46, Asp47 Ser1, Leu66, Leu86
	5-Aminovaleric acid	138	−5.0	x = 7.693 y = 9.921 z = 14.698	size_x = 40 size_y = 40 size_z = 40	Arg106, Gln96, Glu72	Thr60, Ala75, Thr74
	Oleic Acid	445639	−5.0	x = 7.693 y = 9.921 z = 14.698	size_x = 40 size_y = 40 size_z = 40	Leu86	Gly88, Ile49, Val44 Gly46, Asp47, Ile65 Leu66, Asp87
	Linoleic acid	5280450	−4.9	x = 7.693 y = 9.921 z = 14.698	size_x = 40 size_y = 40 size_z = 40	Leu86	Thr85, Leu66, Asp47 Cys1, Gly46, Ser1 Met0
	Palmitic acid	985	−4.4	x = 7.693 y = 9.921 z = 14.698	size_x = 40 size_y = 40 size_z = 40	Glu72, Val80	Lys79, Asp71, Val73 Glu61, Thr60

Table 6. *Cont.*

Protein	Ligand	PubChem ID	Binding Energy (kcal/mol)	Grid Box Center	Grid Box Dimension	Hydrogen Bond Interactions Amino Acid Residue	Hydrophobic Interactions Amino Acid Residue
	(Z)-9-Hexadecenal	5364643	−4.0	x = 7.693 y = 9.921 z = 14.698	size_x = 40 size_y = 40 size_z = 40	N/A	Glu109, Val90, Lys105 Lys107, Val114, Glu116
NR1H3 (PDB ID: 2ACL)	(*) β-Amyrone	612782	−15.4	x = 48.735 y = 39.677 z = 77.096	size_x = 40 size_y = 40 size_z = 40	N/A	Gln330, Ala325, Gly328 Arg248, Arg245, Lys431 Gln297, Leu294, Gln429 Val298, Asp295, Leu329
	β-Stigmasterol	6432745	−11.1	x = 48.735 y = 39.677 z = 77.096	size_x = 40 size_y = 40 size_z = 40	N/A	Gln429, Arg248, Gly328 Leu329, Gln330, Glu332 Ile299, Val331, Arg302 Val298, Asp295, Leu294
	β-Sitosterol	222284	−8.1	x = 48.735 y = 39.677 z = 77.096	size_x = 40 size_y = 40 size_z = 40	Asn385	Pro237, Glu388, Glu322 Ala391, Lys395, Ala398 Leu400, Glu394, Pro240 Lys326, Ile238
	Estradiol, 3-deoxy	537293	−8.0	x = 48.735 y = 39.677 z = 77.096	size_x = 40 size_y = 40 size_z = 40	N/A	Pro240, Leu347, Ala343 Asp379, Ser411, Arg404 Met407, Lys408, Glu390 Glu346
	Sitostenone	5484202	−7.7	x = 48.735 y = 39.677 z = 77.096	size_x = 40 size_y = 40 size_z = 40	Asn385	Glu388, Ala391, Lys395 Pro240, Glu322, Glu394 Leu400, Asp241, Trp236 Pro242, Arg251, Lys326 Ile238, Pro237
	24-epicampesterol	5283637	−7.7	x = 48.735 y = 39.677 z = 77.096	size_x = 40 size_y = 40 size_z = 40	Asn385	Glu388, Ala391, Lys395 Glu394, Asp241, Pro242 Pro240, Lys326, Ile238 Glu322, Pro237
	Ethyl linoleate	5282184	−6.0	x = 48.735 y = 39.677 z = 77.096	size_x = 40 size_y = 40 size_z = 40	N/A	Gln330, Lys381, Ile299 Asp295, Leu294, Lys431 Arg248, Gln429, Val298 Arg302, Gly382
	Linoleic acid	5280450	−5.2	x = 48.735 y = 39.677 z = 77.096	size_x = 40 size_y = 40 size_z = 40	Ser411	Leu347, Arg404, Pro378 Asp379, Ala387, Pro386 Glu390, Pro240, Glu346 Lys408, Ala343
	Oleic Acid	445639	−4.9	x = 48.735 y = 39.677 z = 77.096	size_x = 40 size_y = 40 size_z = 40	N/A	Arg404, Glu390, Lys408 Arg342, Glu339, Pro386 Pro240, Glu346, Tyr397 Met407

(*): The most stable bioactive on a target.

Table 7. Binding energy and interactions of potential bioactives on the PI3K-Akt signaling pathway.

| Protein | Ligand | PubChem ID | Binding Energy (kcal/mol) | Grid Box | | Hydrogen Bond Interactions | Hydrophobic Interactions |
				Center	Dimension	Amino Acid Residue	Amino Acid Residue
AKT1 (PDB ID: 3O96)	(*) Neotocopherol	86052	−6.6	x = 6.313 y = −7.926 z = 17.198	size_x = 40 size_y = 40 size_z = 40	Asn53	Ser56, Ala58, Trp80 Leu213, Phe225, Ser216 Leu223, Phe217, Gln218 Leu78, Gln59, Asn199
IL6 (PDB ID: 4NI9)	(*) Xanthosine	64959	−7.4	x = 11.213 y = 33.474 z = 11.162	size_x = 40 size_y = 40 size_z = 40	Ser37	Asp34, Ala38
	2-Ethylacridine	610161	−6.7	x = 11.213 y = 33.474 z = 11.162	size_x = 40 size_y = 40 size_z = 40	N/A	Asp34, Gly35, Tyr31 Gln111
	Linoleic acid	5280450	−5.0	x = 11.213 y = 33.474 z = 11.162	size_x = 40 size_y = 40 size_z = 40	Lys39	Glu81, Pro80, Ser168 Phe83, Glu105, Leu104 Gln166, Lys103, Glu165 Pro40, Ile106
VEGFA (PDB ID: 3V2A)	(*) Ethyl palmitate	12366	−6.4	x = 38.009 y = −10.962 z = 12.171	size_x = 40 size_y = 40 size_z = 40	N/A	Gly196, Lys48, Ile215 Ile80, Met81, Ile91 Gln79, His133, Pro49 Tyr165
	Ethyl heptadecanoate	26397	−5.1	x = 38.009 y = −10.962 z = 12.171	size_x = 40 size_y = 40 size_z = 40	N/A	Pro40, Asp276, Phe36 Lys48, Phe47, Ile46 Lys286, Asp34
	Ethyl stearate	8122	−5.0	x = 38.009 y = −10.962 z = 12.171	size_x = 40 size_y = 40 size_z = 40	N/A	Gln87, Gly88, Tyr137 Ile138, Lys144, Val146 Ser189, Thr45, Thr139 His86
	Ethyl linoleate	5282184	−4.9	x = 38.009 y = −10.962 z = 12.171	size_x = 40 size_y = 40 size_z = 40	N/A	Pro40, Asp276, Asp34 Phe47, Lys48, Asn253 Ile46, Lys286, Phe36
	α-D-2-deoxyribose	441475	−4.2	x = 38.009 y = −10.962 z = 12.171	size_x = 40 size_y = 40 size_z = 40	Gly255, Ser310, Gly312	Glu44, Asp257, Lys84 Pro85, Ser311
PRKCA (PDB ID: 3IW4)	(*) Ethyl palmitate	12366	−6.4	x = −14.059 y = 38.224 z = 32.319	size_x = 40 size_y = 40 size_z = 40	N/A	Gly196, Met197, Ile80 Met81, Ile91, Gln79 His133, Pro49, Lys48 Tyr165, Ile215
	Ethyl heptadecanoate	26397	−6.2	x = −14.059 y = 38.224 z = 32.319	size_x = 40 size_y = 40 size_z = 40	Lys396	Leu393, Asn660, Gln402 Pro666, Ile667, Glu474 Lys478, Pro398, Val664 Pro397, Arg608

Table 7. *Cont.*

Protein	Ligand	PubChem ID	Binding Energy (kcal/mol)	Grid Box Center	Grid Box Dimension	Hydrogen Bond Interactions Amino Acid Residue	Hydrophobic Interactions Amino Acid Residue
	Ethyl linoleate	5282184	−6.2	x = −14.059 y = 38.224 z = 32.319	size_x = 40 size_y = 40 size_z = 40	Lys396	Asn660, Gln402, Pro666 Val664, Glu418, His665 Arg608, Lys478, Pro398 Asp395, Leu393, Leu394
	2,4,4-Trimethylpentane-1,3-diyl bis(2-methylpropanoate)	93439	−6.0	x = −14.059	size_x = 40	Asp472, His476, Arg608	Ser670, Ile510, Met551
				y = 38.224 z = 32.319	size_y = 40 size_z = 40		Gln548, Glu609, Asp544 Glu552, Ile667, Asn607 Leu668, Glu474
	Linoleic acid	5280450	−5.4	x = −14.059 y = 38.224 z = 32.319	size_x = 40 size_y = 40 size_z = 40	Lys396	Leu393, Pro397, Asn660 Leu394, Ser549, Gln662 Gln548, His553, Glu552 Val664, Pro398, Gln402
	Ethyl stearate	8122	−5.0	x = −14.059 y = 38.224 z = 32.319	size_x = 40 size_y = 40 size_z = 40	N/A	Arg275, Phe36, Asp34 Lys48, Phe47, Ile46 Lys286, Asp276, Pro40
	(Z)-9-Hexadecenal	5364643	−4.2	x = −14.059 y = 38.224 z = 32.319	size_x = 40 size_y = 40 size_z = 40	Asp395, Lys396	Gln402, Pro398, Val664 Glu552, Gln662, Leu394
	Palmitic acid	985	−3.8	x = −14.059 y = 38.224 z = 32.319	size_x = 40 size_y = 40 size_z = 40	Phe47	Phe36, Lys286, Leu252 Leu277, Asp276, Ile46 Asn253, Ser50
	Oleic Acid	445639	−3.5	x = −14.059 y = 38.224 z = 32.319	size_x = 40 size_y = 40 size_z = 40	N/A	Thr145, Val146, Ile138 His86, Leu313, Thr139 Tyr137, Ser189, Lys144
FGF1 (PDB ID: 3OJ2)	(*) Sitostenone	5484202	−8.5	x = 9.051 y = 22.527 z = −0.061	size_x = 40 size_y = 40 size_z = 40	N/A	Arg203, Ser220, Val222 Phe172, Ile257, Ser282 Pro19, Tyr281, Ile204 Ala260
	24-epicampesterol	5283637	−8.3	x = 9.051 y = 22.527 z = −0.061	size_x = 40 size_y = 40 size_z = 40	Ile204	Arg203, Val222, Tyr281 Pro19, Ile257, Ser220 Ala260
	Cytidine	6175	−6.7	x = 9.051 y = 22.527 z = −0.061	size_x = 40 size_y = 40 size_z = 40	Asn350, Arg255, Gln351	Asn107, Asn173, Phe172 Leu258, Ser220, Ala349 Thr174

Table 7. *Cont.*

Protein	Ligand	PubChem ID	Binding Energy (kcal/mol)	Grid Box Center	Grid Box Dimension	Hydrogen Bond Interactions Amino Acid Residue	Hydrophobic Interactions Amino Acid Residue
FGF2 (PDB ID: 1IIL)	α-D-2-deoxyribose	441475	−5.2	x = 9.051	size_x = 40	Gln348, Asn350, Thr174	Ala349, Phe172
				y = 22.527	size_y = 40	Asn173, Asn107, Arg255	
				z = −0.061	size_z = 40		
	(*) β-Amyrone	612782	−14.4	x = 26.785	size_x = 40	N/A	Glu197, Tyr207, Phe198
				y = 14.360	size_y = 40		Lys199, Glu201, Arg118
				z = −1.182	size_z = 40		Gln200, Lys119
	β-Stigmasterol	6432745	−10.9	x = 26.785	size_x = 40	Arg118	Glu201, Asp99, Gln200
				y = 14.360	size_y = 40		Tyr207, Val209, Lys119
				z = −1.182	size_z = 40		
	Sitostenone	5484202	−7.7	x = 26.785	size_x = 40	His254	Ala172, Val222, Ile204
				y = 14.360	size_y = 40		Ser220, Leu258, Gln259
				z = −1.182	size_z = 40		Ala260, Ile257
	24-epicampesterol	5283637	−7.7	x = 26.785	size_x = 40	Ser137	Thr139, Trp123, Lys13
				y = 14.360	size_y = 40		Leu312, Asp336, Tyr340
				z = −1.182	size_z = 40		Ile329, Tyr328, Leu327
							Ser122, Glu323
	β-Sitosterol	222284	−7.2	x = 26.785	size_x = 40	Asp336, Tyr340	Ile329, Leu327, Ser122
				y = 14.360	size_y = 40		Thr319, Lys313, Leu312
				z = −1.182	size_z = 40		Lys292
	Cytidine	6175	−6.4	x = 26.785	size_x = 40	Tyr328, Lys313, Thr319	Pro141, Glu323
				y = 14.360	size_y = 40	Asn318, Ser122	
				z = −1.182	size_z = 40		
	α-D-2-deoxyribose	441475	−4.6	x = 26.785	size_x = 40	Arg255, Phe352	Ala172, Thr174, Ser351
				y = 14.360	size_y = 40		Asn173, His353
				z = −1.182	size_z = 40		
PHLPP1 (not available in the PDB)	(*) Neotocopherol	86052	−7.2	x = 26.785	size_x = 40	N/A	Asn1333, Cys273, Asn700
				y = 14.360	size_y = 40		Ser699, Ser722, Asp745
				z = −1.182	size_z = 40		Asn720, Asp1661, Ile1637
							Tyr764, Leu743, Asn1635
							Cys789, Glu1328, Ser768
							Arg815, Ile1326, Thr1327
							Ile1325

(*): The most stable bioactive on a target.

(**A**)

(**B**)

(**C**)
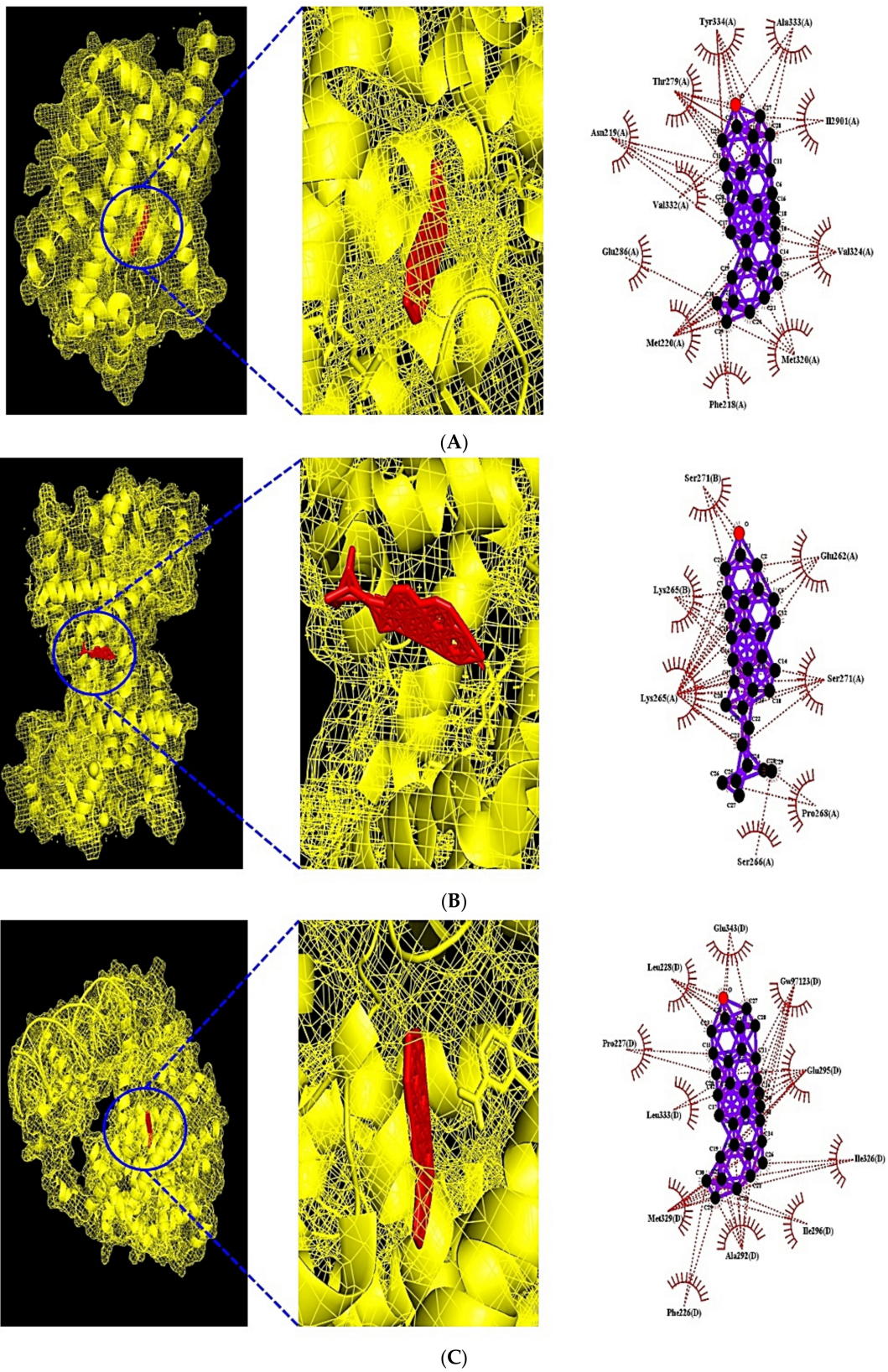
Figure 7. *Cont.*
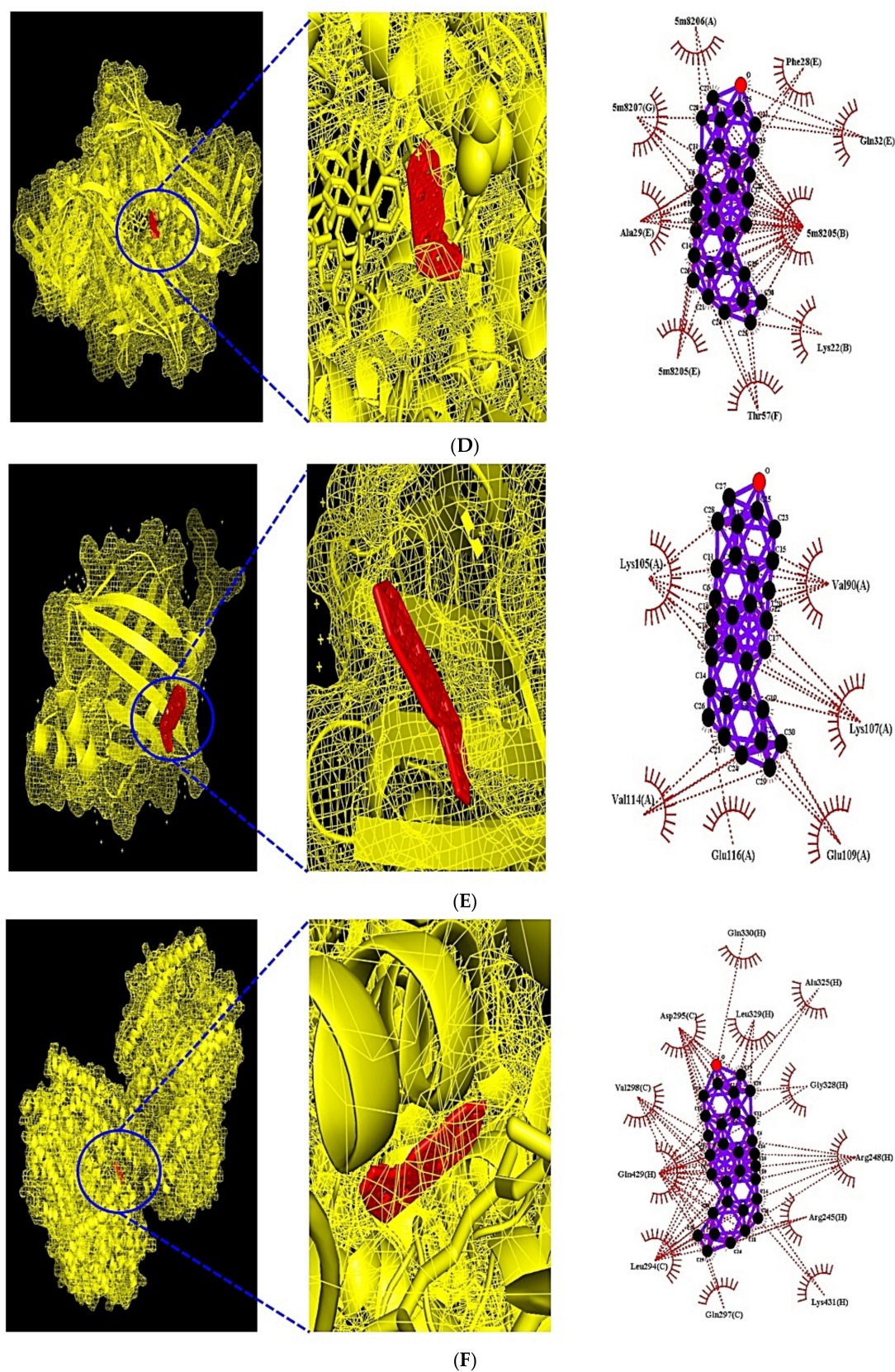
Figure 7. (**A**) MDT of β-Amyrone (PubChem ID: 612782) on PPARA (PDB ID: 3SP6). (**B**) MDT of β-Stigmasterol (PubChem ID: 6432745) on PPARD (PDB ID: 5U3Q). (**C**) MDT of β-Amyrone (PubChem ID: 612782) on PPARG (PDB ID: 3E00). (**D**) MDT of β-Amyrone (PubChem ID: 612782) on FABP3 (PDB ID: 5HZ9). (**E**) MDT of β-Amyrone (PubChem ID: 612782) on FABP4 (PDB ID: 3P6D). (**F**) MDT of β-Amyrone (PubChem ID: 612782) on NR1H3 (PDB ID: 2ACL).

3.8. MDT of 7 Target Proteins, 3 Key Bioactives, and 15 Positive Controls on PI3K-Akt1 Signaling Pathway

Through MDT analysis, it was revealed that AKT1 (PDB ID: 3O96) was related to a sole bioactive: (1) Neotocopherol, IL6 (PDB ID: 4NI9) was associated with 3 bioactives: (1) Xanthosine, (2) 2-Ethylacridine, and (3) Linoleic acid, VEGFA (PDB ID: 3V2A) was connected to (1) Ethyl palmitate, (2) Ethyl heptadecanoate, (3) Ethyl stearate, (4) Ethyl linoleate, and (5) α-D-2-deoxyribose, PRKCA (PDB ID: 3IW4) was linked to 9 bioactives: (1) Ethyl palmitate, (2) Ethyl heptadecanoate, (3) Ethyl linoleate, (4) 2,4,4-Trimethylpentane-1,3-diyl bis(2-methylpropanoate), (5) Linoleic acid, (6) Ethyl stearate, (7) (Z)-9-Hexadecenal, (8) Palmitic acid, and (9) Oleic acid, FGF1 (PDB ID: 3OJ2) was related to 4 bioactives: (1) Sitostenone, (2) 24-epicampesterol, (3) Cytidine, and (4) α-D-2-deoxyribose, FGF2 (PDB ID: 1IIL) was associated with 7 bioactives: (1) β-Amyrone, (2) β-Stigmasterol, (3) Sitostenone, (4) 24-epicampesterol, (5) β-Sitosterol, (6) Cytidine, and (7) α-D-2-deoxyribose, and PHLPP1 was linked to a sole bioactive: (1) Neotocopherol. It was observed that Neotocopherol on AKT1 (PDB ID: 3O96), Xanthosine on IL6 (PDB ID: 4NI9), and β-Amyrone on FGF2 (PDB ID: 1IIL) had the highest affinity among bioactives from CS as well as better affinity than positive controls. The docking detail information is enlisted in Table 8. On the other hand, both Ethyl palmitate had the highest affinity on VEGFA (PDB ID: 3V2A), Sitostenone had the highest affinity on FGF1 (PDB ID: 3OJ2), and lower affinity than BAW2881 and Suramin, which were used as the positive controls, respectively. At present, it was observed that PHLPP1 was not enlisted in PDB, and had valid affinity with β-Amyrone (−7.2 kcal/mol). The detailed affinity value was exhibited in Table 9. The Autodock program was able to assemble active (Gibbs free energy of binding < −6.0 kcal/mol), suggesting that it had highly predictive affinity [37]. Comprehensively, Neotocopherol, Xanthosine, and β-Amyrone of CS on obesity were potential ligands to inhibit PI3K-Akt1 signaling pathway. Its complex figures are depicted in Figure 8.

Table 8. Comparative binding energy between the most stable bioactive(s) and positive control(s) on the PPAR signaling pathway.

Compounds	PubChem ID	Docking Score (kcal/mol)					
		PPARA (PDB ID: 3SP6)	PPARD (PDB ID: 5U3Q)	PPARG (PDB ID: 3E00)	FABP3 (PDB ID: 5HZ9)	FABP4 (PDB ID: 3P6D)	NR1H3 (PDB ID: 2ACL)
β-Amyrone	612782	−16.1					
[1] Clofibrate	2796	−6.4					
[2] Gemfibrozil	3463	−6.3					
[3] Ciprofibrate	2763	−5.4					
[4] Bezafibrate	39042	−5.8					
[5] Fenofibrate	3339	−5.4					
β-Stigmasterol	6432745		−10.8				
[6] Cardarine	9803963		−8.5				
β-Amyrone	612782			−14.0			
[7] Pioglitazone	4829			−7.7			
[8] Rosiglitazone	77999			−7.4			
[9] Lobeglitazone	9826451			−7.3			
β-Amyrone	612782				−21.5		
β-Amyrone	612782					−13.2	
β-Amyrone	612782						−15.4
[10] GW3965	447905						−11.9
[11] T0901317	447912						−8.2

(1)–(5): PPARA agonists, (6): PPARD agonist, (7)–(9): PPARG agonists, (10)–(11): NR1H3 agonists.

Table 9. Comparative binding energy between the most stable bioactive(s) and positive control(s) on the PI3K-Akt signaling pathway.

Compounds	PubChem ID	Docking Score (kcal/mol)						
		AKT1 (PDB ID: 3O96)	IL6 (PDB ID: 4NI9)	VEGFA (PDB ID: 3V2A)	PRKCA (PDB ID: 3IW4)	FGF1 (PDB ID: 3OJ2)	FGF2 (PDB ID: 1IIL)	PHLPP1 (N/A in the PDB)
Neotocopherol	86052	−7.5						
(12) AT13148	24905401	−6.9						
(13) Afuresertib	46843057	−6.9						
(14) Alliin	87310	−4.8						
Xanthosine	64959		−7.4					
(15) APX-115 free base	51036475		−7.2					
(16) Resatorvid	11703255		−7.1					
(17) Myrislignan	21636106		−7.1					
(18) Muscone	10947		−6.7					
(19) 2′,5′-Dihydroxyacetophenone	10279		−6.5					
(20) α-Cyperone	6452086		−6.3					
(21) Veratric acid	7121		−6.1					
(22) Triolein	5497163		−5.5					
(23) Methylthiouracil	667493		−5.4					
(24) Falcarindiol	5281148		−5.2					
Ethyl palmitate	12366			−6.4				
(25) BAW2881	16004702			−7.6				
Ethyl palmitate	12366				−6.4			
(26) Midostaurin	9829523				−11.0			
Sitostenone	5484202					−8.5		
(27) Suramin	5361					−15.4		
β-Amyrone	612782						−14.4	
(28) PD 166866	5328127						−8.3	
Neotocopherol	86052							−7.2

(12)–(14): AKT1 antagonists, (15)–(24): IL6 antagonists, (25): VEGFA antagonist, (26) PRKCA antagonist, (27) FGF1: antagonist, (28) FGF2 antagonist.
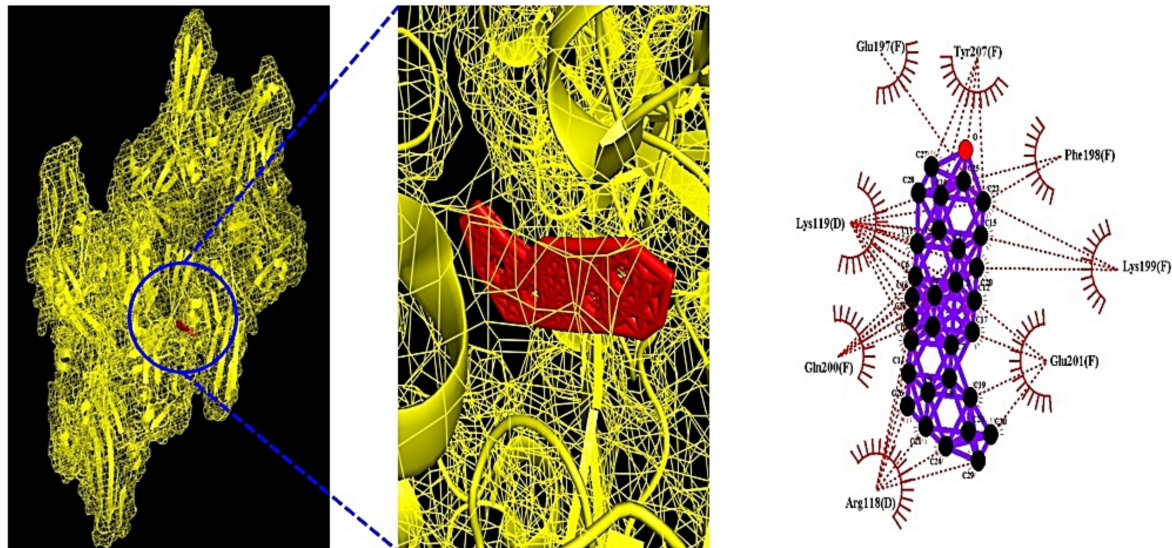
(A)

Figure 8. *Cont.*
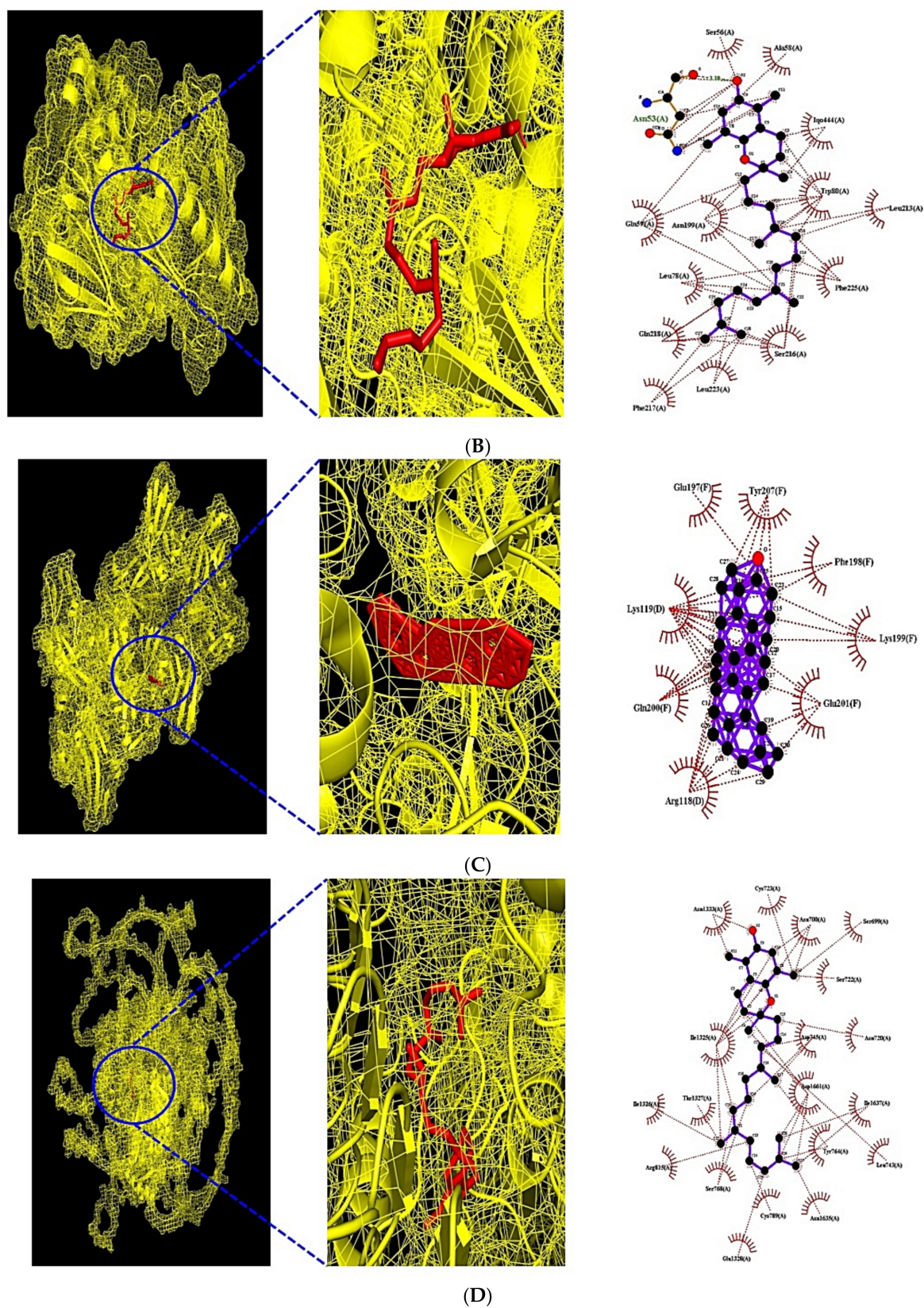
Figure 8. (**A**) MDT of Neotocopherol (PubChem ID: 86052) on AKT1 (PDB ID: 3O96). (**B**) MDT of Xanthosine (PubChem ID: 64959) on IL6 (PDB ID: 4NI9). (**C**) MDT of β-Amyrone (PubChem ID: 612782) on FGF2 (PDB ID: 1IIL). (**D**) MDT of Neotocopherol (PubChem ID: 86052) on PHLPP1.

4. Discussion

β-Amyrone, out of 36 bioactives from CS, was associated with the number of 6 target proteins on both the PPAR signaling pathway and the PI3K-Akt1 signaling pathway, considered as key signaling pathways of CS on obesity. Noticeably, it was unveiled that β-Amyrone (a triterpenoid derivative) on PPARA (PDB ID: 3SP6), PPARG (PDB ID: 3E00) and FGF2 (PDB ID: 1IIL) had better affinity than the positive controls. Likewise, the β-Stigmasterol on PPARD (PDB ID: 5U3Q) had better affinity than Cardarine, which is used as an anti-obesity drug. A report demonstrated that α,β-amyrin, as a triterpenoid derivative homologous to β-Amyrone, inhibits adipocyte differentiation by inactivating PPARG [38]. Another animal test showed that treatment of α,β-amyrin had a significant decrease in the level of blood glucose, serum triglyceride, and total cholesterol [39]. It implies that β-Amyrone might also be a potential ligand to exert an anti-adipogenic effect. A previous study showed that Stigmasterol significantly alleviated high-fat western-style fat (HFWD) induced fatty liver and metabolic disorders, including an increased level of hepatic total lipids, cholesterol, and triacylglycerols [40]. Furthermore, a report demonstrated that the activator of PPARA, PPARD, and PPARG is of great anti-obesity therapeutics due to the regulation of fat and gluconeogenesis [41]. Additionally, a report showed that the NR1H3 agonist makes good efficacy on the enhancement of reverse cholesterol transport, elevation of glucose uptake, and blocking of pro-inflammatory factors [42]. Additionally, Neotocopherol related directly to AKT1, considered as a hub target, had better affinity than two positive controls (AT13148, Afuresertib). There is a noticeable animal study indicating that knock-out of Akt1 elevates energy expenditure and, conversely, decreases the body weight of mice [43]. Another research shows that Akt1 null mice improved their insulin sensitivity and, thereby, elevated insulin secretion [44]. It could be speculated that the inhibitor of Akt1 might play a significant role to attenuate metabolic disorders, including obesity. The Vascular Endothelial Growth Factor A (VEGFA) is overexpressed in obese subjects while inhibitors of VEGF induced anti-proliferation of adipocytes induces weight loss [45,46]. The Fibroblast Growth Factor 2 (FGF2) is elevated in the context of obesity, the disruption of which leads to an increase of thermogenesis with higher energy expenditure and stable lipid maintenance [47,48]. It implies that the inhibitors of VEGFA and FGF2 might be potential ligands against obesity. The STB networks exhibited that the therapeutic effect of CS on obesity was directly associated with 27 bioactives. The KEGG pathway enrichment analysis of 27 bioactives shows that 12 signaling pathways were related to the occurrence and development of obesity, suggesting that these signaling pathways might be the pharmacological mechanisms of ABBR against obesity. The relationships of 12 signaling pathway with obesity were shortly discussed as follows. Advanced Glycation End Product-Receptor for Advanced Glycation End Product (AGE-RAGE) signaling pathway in diabetic complications: the AGE-RAGE signaling pathway influences the oxidative stress related to a diabetic complication, the inhibition of which is a therapeutic strategy for obesity [49,50]. Thyroid hormone signaling pathway: The elevated thyroid hormone levels attenuate the sensitivity of insulin to dampen hepatic glucose production and accelerates the glucose uptake in muscle cells [51]. It has been implicated that excessive thyroid hormone level leads to metabolic disorders, including obesity. Prolactin signaling pathway: It has been documented that prolactin level is increased in obese (17.75 ± 9.15 μg/L) subjects by comparison with subjects of normal weight (13.57 ± 9.03 μg/L) [52]. Estrogen signaling pathway: There is an observational outcome that estrogens play a crucial role in the occurrence of progression of female obesity, primarily via thyroid dysfunction and control of the hypothalamus [53]. Vascular endothelial growth factor (VEGF) signaling pathway: A report shows that inactivation of VEGF enhances the insulin sensitivity in high-fat-diet mice, which is an efficient approach to ameliorate obesity [54]. Phosphoinositide 3-Kinase–Protein Kinase B (PI3K-Akt) signaling pathway: A report demonstrated that inactivation of PI3K alleviates morbid overweight in obese mice and monkeys, indicating that the inhibitors did not induce drug resistance and adverse effects [55]. Additionally, alliin (40 μg/mL) as an inhibitor of Akt, inhibits adipogenesis by downregulating Akt [56].

Hypoxia Inducible Factor-1 (HIF-1) signaling pathway: The attenuation of HIF1-α alleviates glucose intolerance caused by obesity through diminishing Glucagon-Like Peptide-1 (GLP-1) [57]. Cyclic Adenosine MonoPhosphate (cAMP) signaling pathway: the elevation of cAMP level is linked to adipocyte differentiation as a negative factor of severe overweight, berberine known as cAMP inhibitor alleviates anti-obesity by lowering blood glucose, lipid, and body weight [58]. Repressor activator protein 1 (Rap1) signaling pathway: from two groups of mice fed a high fat diet, mice with functional Rap1 gain weight, in contrast, mice that deleted Rap1 remarkably reduced their body weight [59]. Renin-Angiotensin System (RAS) signaling pathway: a research shows that erucin is a bioactive compound isolated from broccoli, known as a Ras inhibitor, and has potent anti-obesity efficacy by inhibiting adipogenesis of 3T3-L1 cell line [60]. Mitogen-Activated Protein Kinase (MAPK) signaling pathway: MAPK, also known as ERK, the inhibition of which is a significant target to alleviate obesity via inhibiting adipogenic differentiation on MAPK signaling pathway [61]. Another research demonstrated that wedelolactone with inhibitory effect on MAPK signaling pathway ablates the adipocyte differentiation [62]. Peroxisome proliferator-activated receptor (PPAR) signaling pathway: a report demonstrated that PPAR activator is therapeutic strategy to alleviate obesity via burning fat brown adipose tissue (BAT), thereby diminishing the fat overload [63].

Besides, our study provided that 11 out 12 signaling pathways associated with AKT1 might have inhibitory effects for the alleviation of obesity, including PI3K-Akt signaling pathway. In contrast, PPAR signaling pathway of CS on obesity is a sole activator mechanism, not related to AKT1. According to a bubble chart, PPI, and STB networks results, we identified 2 signaling pathways, 13 targets, and 27 bioactives, and thus MDT verified that 4 bioactives (β-Amyrone, β-Stigmasterol, Neotocopherol, and Xanthosine) among 27 bioactives could stably bind to the targets, indicating that CS might activate the PPAR signaling pathway, and inactivate PI3K-Akt signaling pathway. Moreover, the final 4 bioactives have better stable affinity than the positive controls. To sum things up, we adopted 2 key signaling pathways (PPAR signaling pathway, PI3K-Akt signaling pathway), 10 targets (PPARA, PPARD, PPARG, FABP3, FABP4, NR1H3, AKT1, IL6, FGF2, and PHLPP1), and 4 bioactives (β-Amyrone, β-Stigmasterol, Neotocopherol, and Xanthosine) (see Figure 9). We removed three complexes (VEGFA-Ethyl palmitate, PRKCA- Ethyl palmitate, and FGF1-Sitostenone) with lower affinity than the positive controls. Hence, in the viewpoint of network pharmacology, this research elucidates promising signaling pathways, targets, and bioactives of CS against obesity, supporting a pharmacological basis for additional experimental validation.
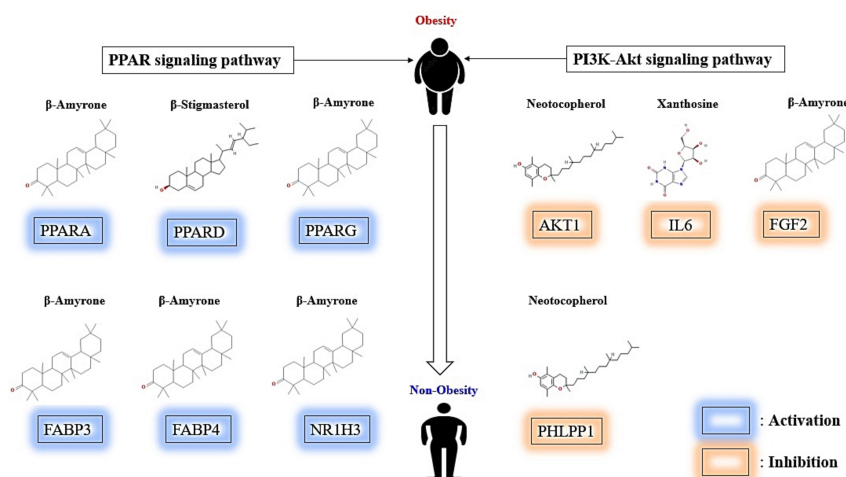
Figure 9. Summary representation of key findings in the study.

5. Conclusions

Overall, this study demonstrated the potential signaling pathways, targets, and bioactives in treating obesity based on network pharmacology analysis. We identified 2 key signaling pathways (PPAR signaling pathway, PI3K-Akt signaling pathway), 13 targets (PPARA, PPARD, PPARG, FABP3, FABP4, NR1H3, AKT1, IL6, VEGFA, PRKCA, FGF1, FGF2, and PHLPP1), and 4 bioactives (β-Amyrone, β-Stigmasterol, Neotocopherol, and Xanthosine) of CS against obesity. A total of 10 out of 13 targets have better affinity or valid value in comparison with the positive controls: PPARA, PPARD, PPARG, FABP3, FABP4, NR1H3, AKT1, IL6, FGF2, and PHLPP1. The AKT1 with the highest degree value was considered as the uppermost target, Neotocopherol was a critical bioactive that was bound most stably to AKT1. Notably, β-Amyrone as an activator could dock well with PPARA, PPARG, FABP3, FABP4, NR1H3 on the PPAR signaling pathway, in contrast, β-Amyrone as an inhibitor could dock stably with FGF2 on the PI3K-Akt signaling pathway. This study shows that β-Amyrone of CS might have dual-efficacy to alleviate obesity. To conclude, we described the therapeutic evidence to expound key signaling pathways, targets, and bioactives of CS against obesity. However, there are still limitations to our analysis, which needs to be further improved, through either in vitro or in vivo. Last but not least, our analysis did not consider the expression of the target gene practically after treating the selected compounds, which should be implemented in the future.

Supplementary Materials: The following are available online at https://www.mdpi.com/article/10.3390/cimb43030133/s1, Table S1: The 154, 466, and 154 targets from SEA, STP, and overlapping targets between SEA and STP, respectively. Table S2: The number of 3028 targets associated with obesity and the number of 85 final targets.

Abbreviations

cAMP	cyclic Adenosine MonoPhosphate;
CS	Corn Silk;
DLCs	Drug Like Compounds (DLCs);
DM	Diabetes Mellitus;
FGF1	Fibroblast Growth Factor 1;
FGF2	Fibroblast Growth Factor 2;
GC-MS	Gas Chromatography Mass Spectrometry;
GLP-1	Glucagon-Like Peptide-1;
HIF-1	Hypoxia Inducible Factor-1;
HFWD	High-Fat Western-style fat Diet;
MAPK	Mitogen-Activated Protein Kinase;
MDT	Molecular Docking Test;
PI3K-Akt	Phosphoinositide 3-Kinase–Protein Kinase B;

PPAR	Peroxisome Proliferator-Activated Receptor;
PPARA	Peroxisome Proliferator-Activated Receptor Alpha;
PPARD	Peroxisome Proliferator-Activated Receptor Delta;
PPARG	Peroxisome Proliferator-Activated Receptor Gamma;
PPI	Protein Protein Interaction (PPI);
Rap1	Repressor activator protein 1;
RAS	Renin Angiotensin System;
SEA	Similarity Ensemble Approach;
STB	Signaling pathways-Targets-Bioactives;
STP	SwissTargetPrediction;
TPSA	Topological Polar Surface Area;
VEGFA	Vascular Endothelial Growth Factor A.

References

1. González Jiménez, E. Obesity: Etiologic and pathophysiological analysis. *Endocrinología y Nutrición* **2013**, *60*, 17–24. [CrossRef] [PubMed]
2. Oh, K.K.; Adnan, M.; Ju, I.; Cho, D.H. A network pharmacology study on main chemical compounds from Hibiscus cannabinus L. leaves. *RSC Adv.* **2021**, *11*, 11062–11082. [CrossRef]
3. Racette, S.B.; Deusinger, S.S.; Deusinger, R.H. Obesity: Overview of Prevalence, Etiology, and Treatment. *Phys. Ther.* **2003**, *83*, 276–288. [CrossRef] [PubMed]
4. Pereira-Lancha, L.O.; Campos-Ferraz, P.L.; Lancha, A.H. Junior Obesity: Considerations about etiology, metabolism, and the use of experimental models. *Diabetes Metab. Syndr. Obes. Targets Ther.* **2012**, *5*, 75. [CrossRef]
5. Kuczmarski, R.J.; Flegal, K.M. Criteria for definition of overweight in transition: Background and recommendations for the United States. *Am. J. Clin. Nutr.* **2000**, *72*, 1074–1081. [CrossRef]
6. Widjaja, N.A.; Prihaningtyas, R.A. Determinants of Food Choice in Obesity. *Indones. J. Public Health* **2020**, *15*, 122–132. [CrossRef]
7. Kelly, T.; Yang, W.; Chen, C.S.; Reynolds, K.; He, J. Global burden of obesity in 2005 and projections to 2030. *Int. J. Obes.* **2008**, *32*, 1431–1437. [CrossRef]
8. Barja-Fernandez, S.; Leis, R.; Casanueva, F.; Seoane, L. Drug development strategies for the treatment of obesity: How to ensure efficacy, safety, and sustainable weight loss. *Drug Des. Dev. Ther.* **2014**, *8*, 2391. [CrossRef]
9. Rodgers, R.J.; Tschöp, M.H.; Wilding, J.P.H. Anti-obesity drugs: Past, present and future. *Dis. Models Mech.* **2012**, *5*, 621. [CrossRef]
10. Heck, D.A.M.; Yanovski, D.J.A.; Calis, D.K.A. Orlistat, a New Lipase Inhibitor for the Management of Obesity. *Pharmacotherapy* **2000**, *20*, 270. [CrossRef] [PubMed]
11. Li, M.; Cheung, B.M.Y. Pharmacotherapy for obesity. *Br. J. Clin.Pharmacol.* **2009**, *68*, 804. [CrossRef]
12. Derosa, G.; Maffioli, P. Anti-obesity drugs: A review about their effects and their safety. *Expert Opin. Drug Saf.* **2012**, *11*, 459–471. [CrossRef] [PubMed]
13. Zhang, J.; Onakpoya, I.J.; Posadzki, P.; Eddouks, M. The safety of herbal medicine: From prejudice to evidence. *Evid. Based Complementary Altern. Med.* **2015**, *2015*, 316706. [CrossRef]
14. Watanabe, T. Therapeutic properties of the new phytochemical osmotin for preventing atherosclerosis. *Vessel Plus* **2020**, *4*, 4. [CrossRef]
15. Jo, M.G.; Kim, M.W.; Jo, M.H.; bin Abid, N.; Kim, M.O. Adiponectin homolog osmotin, a potential anti-obesity compound, suppresses abdominal fat accumulation in C57BL/6 mice on high-fat diet and in 3T3-L1 adipocytes. *Int. J. Obes.* **2019**, *43*, 2422–2433. [CrossRef]
16. Shaji, J.; Patole, V. Protein and Peptide Drug Delivery: Oral Approaches. *Indian J. Pharm. Sci.* **2008**, *70*, 269. [CrossRef]
17. Pérez, M.; Pérez, D.I.; Martínez, A.; Castro, A.; Gómez, G.; Fall, Y. The first enantioselective synthesis of palinurin. *Chem. Commun.* **2009**, *22*, 3252–3254. [CrossRef]
18. Zhang, Y.; Li, Y.; Guo, Y.; Jiang, H.; Shen, X. A sesquiterpene quinone, dysidine, from the sponge Dysidea villosa, activates the insulin pathway through inhibition of PTPases. *Acta Pharmacol. Sin.* **2009**, *30*, 333–345. [CrossRef]
19. Noinart, J.; Buttachon, S.; Dethoup, T.; Gales, L.; Pereira, J.A.; Urbatzka, R.; Freitas, S.; Lee, M.; Silva, A.M.S.; Pinto, M.M.M.; et al. A New Ergosterol Analog, a New Bis-Anthraquinone and Anti-Obesity Activity of Anthraquinones from the Marine Sponge-Associated Fungus Talaromyces stipitatus KUFA 0207. *Mar. Drugs* **2017**, *15*, 139. [CrossRef]
20. Seo, Y.J.; Lee, K.T.; Rho, J.R.; Choi, J.H. Phorbaketal A, Isolated from the Marine Sponge Phorbas sp., Exerts Its Anti-Inflammatory Effects via NF-κB Inhibition and Heme Oxygenase-1 Activation in Lipopolysaccharide-Stimulated Macrophages. *Mar. Drugs* **2015**, *13*, 7005–7019. [CrossRef] [PubMed]
21. Karri, S.; Sharma, S.; Hatware, K.; Patil, K. Natural anti-obesity agents and their therapeutic role in management of obesity: A future trend perspective. *Biomed. Pharmacother.* **2019**, *110*, 224–238. [CrossRef]
22. Chaiittianan, R.; Chayopas, P.; Rattanathongkom, A.; Tippayawat, P.; Sutthanut, K. Anti-obesity potential of corn silks: Relationships of phytochemicals and antioxidation, anti-pre-adipocyte proliferation, anti-adipogenesis, and lipolysis induction. *J. Funct. Foods* **2016**, *23*, 497–510. [CrossRef]

23. Cosme, P.; Rodríguez, A.B.; Espino, J.; Garrido, M. Plant Phenolics: Bioavailability as a Key Determinant of Their Potential Health-Promoting Applications. *Antioxidants* **2020**, *9*, 1263. [CrossRef]

24. Chen, Y.; Bi, F.; Sun, Z. A network pharmacology approach to determine the underlying mechanisms of action of Yishen Tongluo formula for the treatment of oligoasthenozoospermia. *PLoS ONE* **2021**, *16*, e0252906. [CrossRef]

25. Li, W.; Yuan, G.; Pan, Y.; Wang, C.; Chen, H. Network Pharmacology Studies on the Bioactive Compounds and Action Mechanisms of Natural Products for the Treatment of Diabetes Mellitus: A Review. *Front. Pharmacol.* **2017**, *8*, 74. [CrossRef]

26. Shi, S.; Cai, Y.; Cai, X.; Zheng, X.; Cao, D.; Ye, F.; Xiang, Z. A Network Pharmacology Approach to Understanding the Mechanisms of Action of Traditional Medicine: Bushenhuoxue Formula for Treatment of Chronic Kidney Disease. *PLoS ONE* **2014**, *9*, e89123. [CrossRef] [PubMed]

27. Oh, K.K.; Adnan, M.; Cho, D.H. A network pharmacology analysis on drug-like compounds from Ganoderma lucidum for alleviation of atherosclerosis. *J. Food Biochem.* **2021**, *45*, e13906. [CrossRef]

28. Matsson, P.; Kihlberg, J. How Big Is Too Big for Cell Permeability? *J. Med. Chem.* **2017**, *60*, 1662–1664. [CrossRef] [PubMed]

29. Kaiser, M.J.; Roth, B.L.; Armbruster, B.N.; Ernsberger, P.; Irwin, J.J.; Schoichet, B.K. Relating protein pharmacology by ligand chemistry. *Nat. Biotechnol.* **2007**, *25*, 197–206. [CrossRef] [PubMed]

30. Daina, A.; Michielin, O.; Zoete, V. SwissTargetPrediction: Updated data and new features for efficient prediction of protein targets of small molecules. *Nucleic Acids Res.* **2019**, *47*, W357. [CrossRef] [PubMed]

31. Singh, N.; Chaput, L.; Villoutreix, B.O. Virtual screening web servers: Designing chemical probes and drug candidates in the cyberspace. *Brief. Bioinform.* **2021**, *22*, 1790–1818. [CrossRef]

32. Soo, H.-C.; Chung, F.F.-L.; Lim, K.-H.; Yap, V.A.; Bradshaw, T.D.; Hii, L.-W.; Tan, S.-H.; See, S.-J.; Tan, Y.-F.; Leong, C.-O.; et al. Cudraflavone C Induces Tumor-Specific Apoptosis in Colorectal Cancer Cells through Inhibition of the Phosphoinositide 3-Kinase (PI3K)-AKT Pathway. *PLoS ONE* **2017**, *12*, e0170551. [CrossRef] [PubMed]

33. Heberle, H.; Meirelles, G.V.; da Silva, F.R.; Telles, G.P.; Minghim, R. InteractiVenn: A web-based tool for the analysis of sets through Venn diagrams. *BMC Bioinform.* **2015**, *16*, 169. [CrossRef]

34. Szklarczyk, D.; Gable, A.L.; Lyon, D.; Junge, A.; Wyder, S.; Huerta-Cepas, J.; Simonovic, M.; Doncheva, N.T.; Morris, J.H.; Bork, P.; et al. STRING v11: Protein–protein association networks with increased coverage, supporting functional discovery in genome-wide experimental datasets. *Nucleic Acids Res.* **2019**, *47*, D607–D613. [CrossRef] [PubMed]

35. Khanal, P.; Patil, B.M.; Chand, J.; Naaz, Y. Anthraquinone Derivatives as an Immune Booster and their Therapeutic Option Against COVID-19. *Nat. Prod. Bioprospect.* **2020**, *10*, 325. [CrossRef] [PubMed]

36. Laskowski, R.A.; Swindells, M.B. LigPlot$^+$: Multiple ligand-protein interaction diagrams for drug discovery. *J. Chem. Inf. Modeling* **2011**, *51*, 2778–2786. [CrossRef] [PubMed]

37. Shityakov, S.; Förster, C. In silico predictive model to determine vector-mediated transport properties for the blood–brain barrier choline transporter. *Adv. Appl. Bioinform. Chem. AABC* **2014**, *7*, 23. [CrossRef] [PubMed]

38. De Melo, K.M.; de Oliveira, F.T.B.; Costa Silva, R.A.; Gomes Quinderé, A.L.; Marinho Filho, J.D.B.; Araújo, A.J.; Barros Pereira, E.D.; Carvalho, A.A.; Chaves, M.H.; Rao, V.S.; et al. α, β-Amyrin, a pentacyclic triterpenoid from *Protium heptaphyllum* suppresses adipocyte differentiation accompanied by down regulation of PPARγ and C/EBPα in 3T3-L1 cells. *Biomed. Pharmacother.* **2019**, *109*, 1860–1866. [CrossRef]

39. Santos, F.A.; Frota, J.T.; Arruda, B.R.; de Melo, T.S.; de Castro Brito, G.A.; Chaves, M.H.; Rao, V.S. Antihyperglycemic and hypolipidemic effects of α, β-amyrin, a triterpenoid mixture from *Protium heptaphyllum* in mice. *Lipids Health Dis.* **2012**, *11*, 1–8. [CrossRef]

40. Feng, S.; Dai, Z.; Liu, A.B.; Huang, J.; Narsipur, N.; Guo, G.; Kong, B.; Reuhl, K.; Lu, W.; Luo, Z.; et al. Intake of stigmasterol and β-sitosterol alters lipid metabolism and alleviates NAFLD in mice fed a high-fat western-style diet. *Biochim. Biophys. Acta Mol. Cell Biol. Lipids* **2018**, *1863*, 1274–1284. [CrossRef] [PubMed]

41. Moller, D.E.; Berger, J.P. Role of PPARs in the regulation of obesity-related insulin sensitivity and inflammation. *Int. J. Obes.* **2003**, *27* (Suppl. S3), S17–S21. [CrossRef]

42. Laurencikiene, J.; Rydén, M. Liver X receptors and fat cell metabolism. *Int. J. Obes.* **2012**, *36*, 1494. [CrossRef]

43. Wan, M.; Easton, R.M.; Gleason, C.E.; Monks, B.R.; Ueki, K.; Kahn, C.R.; Birnbaum, M.J. Loss of Akt1 in mice increases energy expenditure and protects against diet-induced obesity. *Mol. Cell. Biol.* **2012**, *32*, 96–106. [CrossRef]

44. Buzzi, F.; Xu, L.; Zuellig, R.A.; Boller, S.B.; Spinas, G.A.; Hynx, D.; Chang, Z.; Yang, Z.; Hemmings, B.A.; Tschopp, O.; et al. Differential Effects of Protein Kinase B/Akt Isoforms on Glucose Homeostasis and Islet Mass. *Mol. Cell. Biol.* **2010**, *30*, 601. [CrossRef]

45. Nijhawans, P.; Behl, T.; Bhardwaj, S. Angiogenesis in obesity. *Biomed. Pharmacother.* **2020**, *126*, 110103. [CrossRef] [PubMed]

46. Ngo, D.T.; Farb, M.G.; Kikuchi, R.; Karki, S.; Tiwari, S.; Bigornia, S.J.; Bates, D.O.; LaValley, M.P.; Hamburg, N.M.; Vita, J.A.; et al. Anti-Angiogenic Actions of VEGF-A165b, an Inhibitory Isoform of VEGF-A, in Human Obesity. *Circulation* **2014**, *130*, 1072. [CrossRef] [PubMed]

47. Boothby-Shoemaker, W.; Benham, V.; Paithankar, S.; Shankar, R.; Chen, B.; Bernard, J.J. The Relationship between Leptin, the Leptin Receptor and FGFR1 in Primary Human Breast Tumors. *Cells* **2020**, *9*, 2224. [CrossRef] [PubMed]

48. Li, H.; Zhang, X.; Huang, C.; Liu, H.; Liu, S.; Zhang, Q.; Dong, M.; Hou, M.; Liu, Y.; Lin, H. FGF2 disruption enhances thermogenesis in brown and beige fat to protect against obesity and hepatic steatosis. *bioRxiv* **2020**. [CrossRef]

49. Kay, A.M.; Simpson, C.L.; Stewart, J.A. The Role of AGE/RAGE Signaling in Diabetes-Mediated Vascular Calcification. *J. Diabetes Res.* **2016**, *2016*, 6809703. [CrossRef]

50. Sellegounder, D.; Zafari, P.; Rajabinejad, M.; Taghadosi, M.; Kapahi, P. Advanced glycation end products (AGEs) and its receptor, RAGE, modulate age-dependent COVID-19 morbidity and mortality. A review and hypothesis. *Int. Immunopharmacol.* **2021**, *98*, 107806. [CrossRef]

51. Bandurska-Stankiewicz, E. Thyroid hormones—Obesity and metabolic syndrome. *Thyroid Res.* **2013**, *6*, A5. [CrossRef]

52. Bernard, V.; Young, J.; Binart, N. Prolactin—A pleiotropic factor in health and disease. *Nat. Rev. Endocrinol.* **2019**, *15*, 356–365. [CrossRef] [PubMed]

53. Grantham, J.P.; Henneberg, M. The Estrogen Hypothesis of Obesity. *PLoS ONE* **2014**, *9*, e99776. [CrossRef] [PubMed]

54. Wu, L.E.; Meoli, C.C.; Mangiafico, S.P.; Fazakerley, D.J.; Cogger, V.C.; Mohamad, M.; Pant, H.; Kang, M.-J.; Powter, E.; Burchfield, J.G.; et al. Systemic VEGF-A Neutralization Ameliorates Diet-Induced Metabolic Dysfunction. *Diabetes* **2014**, *63*, 2656–2667. [CrossRef] [PubMed]

55. Ortega-Molina, A.; Lopez-Guadamillas, E.; De Cabo, R.; Serrano, M. Pharmacological Inhibition of PI3K Reduces Adiposity and Metabolic Syndrome in Obese Mice and Rhesus Monkeys. *Cell Metab.* **2015**, *21*, 558–570. [CrossRef]

56. Li, N.; Chen, K.; Dong, H.; Yang, J.; Yoshizawa, M.; Kagami, H.; Li, X. Alliin inhibits adipocyte differentiation by downregulating Akt expression: Implications for metabolic disease. *Exp. Ther. Med.* **2021**, *21*, 1–8. [CrossRef]

57. Lee, Y.S.; Riopel, M.; Cabrales, P.; Bandyopadhyay, G.K. Hepatocyte-specific HIF-1 ablation improves obesity-induced glucose intolerance by reducing first-pass GLP-1 degradation. *Sci. Adv.* **2019**, *5*, eaaw4176. [CrossRef] [PubMed]

58. Zhang, J.; Tang, H.; Deng, R.; Wang, N.; Zhang, Y.; Wang, Y.; Liu, Y.; Li, F.; Wang, X.; Zhou, L. Berberine Suppresses Adipocyte Differentiation via Decreasing CREB Transcriptional Activity. *PLoS ONE* **2015**, *10*, e0125667. [CrossRef] [PubMed]

59. Kaneko, K.; Xu, P.; Cordonier, E.L.; Chen, S.S.; Ng, A.; Xu, Y.; Morozov, A.; Fukuda, M. Neuronal Rap1 Regulates Energy Balance, Glucose Homeostasis, and Leptin Actions. *Cell Rep.* **2016**, *16*, 3003–3015. [CrossRef]

60. Chae, S.Y.; Seo, S.G.; Yang, H.; Yu, J.G.; Suk, S.J.; Jung, E.S.; Ji, H.; Kwon, J.Y.; Lee, H.J.; Lee, K.W. Anti-adipogenic effect of erucin in early stage of adipogenesis by regulating Ras activity in 3T3-L1 preadipocytes. *J. Funct. Foods* **2015**, *19*, 700–709. [CrossRef]

61. Oh, J.H.; Karadeniz, F.; Lee, J.I.; Seo, Y.; Kong, C.-S. Artemisia princeps Inhibits Adipogenic Differentiation of 3T3-L1 Pre-Adipocytes via Downregulation of PPARγ and MAPK Pathways. *Prev. Nutr. Food Sci.* **2019**, *24*, 299. [CrossRef] [PubMed]

62. Lim, S.; Jang, H.-Y.; Park, E.H.; Kim, J.K.; Kim, J.-M.; Kim, E.-K.; Yea, K.; Kim, Y.-H.; Lee-Kwon, W.; Ryu, S.H.; et al. Wedelolactone inhibits adipogenesis through the ERK pathway in human adipose tissue-derived mesenchymal stem cells. *J. Cell. Biochem.* **2012**, *113*, 3436–3445. [CrossRef] [PubMed]

63. Gross, B.; Pawlak, M.; Lefebvre, P.; Staels, B. PPARs in obesity-induced T2DM, dyslipidaemia and NAFLD. *Nat. Rev. Endocrinol.* **2016**, *13*, 36–49. [CrossRef] [PubMed]